

Beyond Uncertainty Sets: Leveraging Optimal Transport to Extend Conformal Predictive Distribution to Multivariate Settings

Eugene Ndiaye
Apple

Abstract

Conformal prediction (CP) constructs uncertainty sets for model outputs with finite-sample coverage guarantees, all without distributional assumptions other than exchangeability. A candidate output is included in the prediction set if its non-conformity score is not considered extreme relative to the scores observed on a set of calibration examples. However, this procedure is only straightforward when scores are scalar-valued, which has limited CP to real-valued scores or ad-hoc reductions to one dimension. This limitation is critical, as vector-valued scores arise naturally in important settings such as multi-output regression or situations involving model aggregation, where each predictor in an ensemble provides its own score. The problem of ordering vectors has been studied via optimal transport (OT), which provides a principled method for defining vector-ranks and (center-outward) multivariate quantile regions, though typically with only asymptotic coverage guarantees. Specifically, this loss of validity occurs because applying a single, fixed transport map, learned from finite data, to new test points introduces an uncontrolled approximation error. We restore finite-sample, distribution-free coverage by conformalizing the vector-valued OT quantile region. In our approach, a candidate’s rank is defined via a transport map computed for the calibration scores augmented with that candidate’s score—a step crucial for preserving validity. This defines a continuum of OT problems (one for each candidate) which appears computationally infeasible. However, we prove that the resulting optimal assignment is piecewise-constant across a fixed polyhedral partition of the score space. This allows us to characterize the entire prediction set tractably and, crucially, provides the machinery to address a deeper limitation of prediction sets: that they only indicate which outcomes are plausible, but not their relative likelihood. In one dimension, conformal predictive distributions (CPDs) fill this gap by producing a predictive distribution with finite-sample calibration. Extending CPDs beyond one dimension remained an open problem. We construct, to our knowledge, the first multivariate CPDs with finite-sample calibration, i.e., they define a valid multivariate (center-outward) distribution where any derived uncertainty region automatically has guaranteed (conformal) coverage. We present both conservative and exact randomized versions, the latter resulting in a multivariate generalization of the classical Dempster-Hill procedure.

Contents

1	Introduction	2
1.1	Contributions Overview	5
1.2	Related Work	5
2	From Prediction Sets to Predictive Distributions: the Univariate Case	6
2.1	Prediction Sets from the Ground-Truth Distribution	6
2.2	Prediction Sets from the Empirical Distribution	7
2.2.1	Using Uniform Convergence of Empirical Distribution	7
2.2.2	The Conformal Approach	7
2.3	Predictive Distribution Based on Confidence Distribution	9
2.3.1	Bayesian Predictive Distribution	9

2.3.2	Validity Requirement on Predictive Distributions	10
2.4	Conformal Predictive Distributions	11
3	Multivariate Outputs and Vector-Valued Scores	13
3.1	Examples of Vector-Valued Score Function	13
3.2	Multivariate Quantile Region Based on Optimal Transport	14
3.2.1	Quantile Region from the Ground-Truth Distribution	15
3.2.2	Validity Loss due to Approximations	16
4	Multivariate Conformal Prediction via Optimal Transport	17
4.1	Conformalized Quantile Region	17
4.1.1	Augmented Transport Map	17
4.1.2	Coverage Guarantee	18
4.2	Multivariate Prediction Set	19
4.3	A Tractable Algorithm via Polyhedral Partitions	19
4.4	Boundness and Computation of the Quantile Region	21
4.5	Multivariate Predictive Distribution	21
5	Randomized Conformal Predictive Distribution and Generalization of the Dempster-Hill Procedure	24
5.1	One Dimensional Dempster-Hill	24
5.2	Multivariate Dempster-Hill via Semi-Discrete Optimal Transport	26
5.3	Semi-discrete Assignment Stream and Randomized Transport	27
5.3.1	Monotonicity of the Semi-discrete Assignment Stream	28
5.3.2	Boundedness and Computation of the Semi-Discrete Quantile Region	29
6	Discussion and Future Work	30

1 Introduction

Conformal prediction (CP) (Gammerman et al., 1998; Vovk et al., 2005; Shafer and Vovk, 2008) provides a rigorous, model-agnostic framework for quantifying uncertainty. It transforms any point predictor into one that outputs a prediction set, guaranteed to contain the true outcome with a user-specified probability. Ideally, one could interpret the size of this set adapts to the model’s instance-wise difficulty; if the model is inaccurate or uncertain for a given input, the set must grow larger to maintain coverage, whereas for confident predictions, the set can be small. Once coverage is guaranteed to hold, the set’s size thus becomes a data-driven measure of uncertainty. This is achieved without strong assumptions about the underlying data distribution, other than exchangeability. In the most common split-conformal setup, a model \hat{y} is first fitted on a training set; here we consider a supervised learning setting where we observe a sequence of input-output pairs in $\mathcal{X} \times \mathcal{Y}$. Its uncertainty is then calibrated on a separate calibration set

$$D_n = \{(x_1, y_1), \dots, (x_n, y_n)\}.$$

The core of CP is a user-defined non-conformity score function,

$$S(x, y; \hat{y}) \in \mathbb{R},$$

designed to measure the disagreement between a model’s prediction and an observed outcome. The intuition is that a candidate output is considered "strange" if it would cause the model to make an error that is unusually large compared to the errors seen on the calibration data. For example, in regression a common choice is the magnitude of the residual error, $S(x, y; \hat{y}) = |y - \hat{y}(x)|$. The central mechanism of CP addresses the fact that the true label y_{n+1} for a new input x_{n+1} is

unknown. The procedure must therefore systematically consider every possible candidate value $z \in \mathcal{Y}$ that the unknown label could take. For each candidate z , it evaluates whether that choice is plausible by comparing its non-conformity score to the distribution of scores from the calibration data. The final prediction set is simply the collection of all candidates deemed plausible.

The Challenge of Vector-Valued Scores While CP is well-established for scalar-valued score functions as previously discussed, extending it to vector-valued scores

$$S(x, y; \hat{y}) \in \mathbb{R}^d$$

poses a fundamental challenge. The core difficulty is that CP’s mechanism relies on ranking scores, yet there is no unique or canonical way to order vectors in \mathbb{R}^d . This raises the question:

How can we generalize conformal prediction to handle vector-valued scores while preserving its coverage guarantees?

This issue arises in several common machine learning settings. In multivariate regression, a natural score is the full vector of residuals, which captures the error’s direction and magnitude in each output dimension. In classification, while a common scalar score measures the model’s confidence in the true class, it is a lossy summary that discards information about how the probability mass is distributed among the incorrect classes. To preserve this richer information, one can work directly with the full vector of predicted class probabilities. A natural vector-valued score can then be formed from the difference between this probability vector and a one-hot vector representing the true label. Furthermore, even when the response is univariate, vector-valued scores arise in model aggregation. Here, the individual prediction errors from an ensemble of models can be concatenated into a single score vector, representing the collective judgment and disagreement of the ensemble. A naive solution might be to reduce these vectors to a single scalar (e.g., by taking a norm), but doing so can discard important directional or structural information, an issue we discuss in detail in Section 3.

Beyond Prediction Sets The central question posed at the beginning of this section motivates a move beyond simple prediction sets:

How likely is a particular output within the conformal prediction set?

A standard conformal prediction set does not directly answer this question. Among the plausible outcomes, the set itself offers no further information to distinguish their relative likelihoods. This information gap, as highlighted by Hullman et al. (2025), contrasts sharply with calibrated predictive distributions, which provide a granular likelihood for each outcome that can directly guide decision-making. Consequently, prediction sets could be best suited for conservative maximizing worst-case utility (Kiyani et al., 2025), a strategy that may not align with many practical applications. To overcome this limitation, conformal predictive distributions (CPDs) have been developed for the univariate case. A CPD is a full probability distribution over the outcome space that is calibrated in a finite-sample sense: any prediction set derived from it by selecting a region of a certain probability mass automatically has valid conformal coverage. This provides the flexibility of a full distribution and the rigor of a finite-sample guarantee. However, just as with prediction sets, extending CPDs beyond the one-dimensional setting has remained an open problem. This leaves a critical gap: there is no assumption-free method to generate calibrated predictive distributions for the multivariate tasks discussed previously.

Calibrated Predictive Distributions A natural way to quantify predictive uncertainty is to place a full probability distribution over the output space. The Bayesian framework, for instance, provides a principled way to do this via the posterior predictive distribution (Box, 1980; Rubin,

1984; Gelman et al., 1996). However, a well-known challenge is that prediction sets derived from Bayesian posteriors do not, in general, guarantee the desired *frequentist coverage* without strong assumptions about the model being well-specified. This disconnect has motivated work aiming to bridge Bayesian inference and frequentist guarantees. For example, Fong and Holmes (2021) proposed using components of the Bayesian posterior as a scalar non-conformity score within the standard CP framework, thereby achieving valid prediction sets. While effective, this approach still produces only a set, not a fully calibrated predictive distribution. The question of what makes a predictive distribution "good" has a rich history. As emphasized by Dawid (1984) and Diebold et al. (1997), predictive distributions should be evaluated based on the joint behavior of forecast-observation pairs. A key diagnostic for this is the probability integral transform (PIT), which checks for probabilistic calibration (Hamill, 2001; Gneiting et al., 2007). Building on this foundation, Shen et al. (2018) formalized the requirements for what they call a *valid* predictive distribution into two key desiderata:

- (i) For each new input, the procedure must return a proper cumulative distribution function.
- (ii) It must achieve finite-sample calibration.

Here, the core requirement of calibration, means that the predictive probabilities are correct on average for designing uncertainty sets. Intuitively, if the distribution states there is a 70% probability that an outcome lies below a threshold, this event should occur 70% of the time in repeated experiments. More formally, if $F_{Y_{n+1}}$ is the predicted CDF for the outcome Y_{n+1} , a natural calibration property requires that the probability integral transform (PIT) value, $U = F_{Y_{n+1}}(Y_{n+1})$, is a uniform random variable. That is, for all $\alpha \in [0, 1]$, $\mathbb{P}(F_{Y_{n+1}}(Y_{n+1}) \leq \alpha) = \alpha$. This property guarantees that any $(1 - \alpha)$ prediction interval derived from the CDF, such as $[F_{Y_{n+1}}^{-1}(\alpha/2), F_{Y_{n+1}}^{-1}(1 - \alpha/2)]$, will have a $(1 - \alpha)$ coverage. Existing methods that aim for such frequentist guarantees, like those of Lawless and Fredette (2005) and Shen et al. (2018), typically achieve them by assuming a correctly specified model or other regularity conditions. This leaves a critical gap and motivates another central question:

Can we construct a predictive distribution that satisfies the desiderata of calibration and correctness for any finite sample, but without relying on assumptions about the model or data distribution?

Conformal Predictive Distributions (CPDs) Just as the original conformal framework elevates a point predictor into one that outputs a prediction set, Conformal Predictive Distributions (CPDs) complete this evolution by transforming the point predictor into a full, calibrated predictive distribution over the outcome space. This nice extension was introduced by Vovk et al. (2017); Vovk and Bendtsen (2018); Vovk (2019) for the univariate setting. The method provides a constructive, distribution-free way to generate a calibrated predictive distribution, typically by converting the conformal p-values or ranks into a valid CDF. The resulting distribution retains the rigorous finite-sample guarantees of conformal methods while offering a granular, probability-based representation of uncertainty that is more naturally suited for risk-sensitive decision-making. Despite this conceptual power, the application of CPDs has been severely limited to one dimensional settings despite some growing interest in the framework. Recent benchmarks have demonstrated the practical advantages of CPDs over classical Bayesian predictive distributions (Lanngren et al., 2025), and new applications are emerging in areas like Gaussian processes (Pion and Vazquez, 2025). Extending CPDs to multivariate outputs, however, faces the same fundamental ordering problem as prediction sets and has remained an open challenge since at least Vovk and Bendtsen (2018). This leaves a critical gap: there is no distribution-free method to provide a combination of a full predictive distribution and a rigorous finite-sample guarantee for the multivariate tasks discussed previously.

1.1 Contributions Overview

We address two core gaps in conformal prediction for multivariate settings: (i) how to construct valid prediction sets for vector-valued scores, and (ii) how to build conformal multivariate predictive distributions. We summarize our contributions as follows:

- *Conformal Prediction with Vector-Valued Score.* We provide an extension of conformal prediction to vector-valued scores that retains exact, finite-sample, distribution-free coverage. Our key theoretical insight is to "conformalize" the ranking process by defining a candidate's rank via an optimal transport map computed on an *augmented sample* that includes the candidate itself. This ensures that the exchangeability required for the conformal guarantee is fully maintained for test points.
- *A Tractable Algorithm.* Our approach defines a continuum of OT problem (one for each candidate), which is computationally infeasible at first sight. We solve this by proving that the optimal assignment function is piecewise-constant across a fixed polyhedral partition of the score space. This insight allows us to develop a tractable algorithm that pre-computes this partition once, reducing the problem of characterizing the entire prediction set to a fast cell lookup at test time. This avoids re-solving a new OT problems for infinitely many candidates; which is untractable.
- *Multivariate Conformal Predictive Distributions (CPDs).* Building on the two previous point, we construct a multivariate CPDs with finite-sample calibration. This provide a solution to an important problem that was left open since at least (Vovk and Bendtsen, 2018) and provides, to our knowledge, a first multivariate generalization of the classical Dempster–Hill procedure (Dempster, 1963). This final contribution benefits directly from the tractability of the algorithm developed in our second contribution.

1.2 Related Work

Work on multivariate uncertainty for conformal prediction has followed several practical paths. We briefly review the main lines; further discussion and implementation details appear in the appendix. The approaches in this paper avoids learning a global transport map, includes the test candidate within a discrete OT formulation to retain exact finite-sample guarantees, removes the need to solve OT per candidate by exploiting a polyhedral partition of score space, and provides, to our knowledge, the first multivariate CPDs with finite-sample calibration.

Scalarizing vector scores with norms. A straightforward approach reduces a vector of residuals to a single number using a norm, so that standard (univariate) conformal prediction can be applied "as is." Variants first re-scale or whiten the coordinates to account for different scales and correlations across targets, for example by using a Mahalanobis-type norm (Johnstone and Cox, 2021; Messoudi et al., 2022). More recent work learns an ellipsoidal shape to shrink the prediction sets while preserving coverage (Braun et al., 2025). Dheur et al. (2025) presents a large benchmark.

Optimal-transport merging with a pre-fit transform. A pragmatic alternative learns a fixed transport map on a hold-out split that sends multivariate scores to a simple reference distribution, and then calibrates a scalar summary of the transformed scores with standard conformal prediction (Thurin et al., 2025; Klein et al., 2025). To maintain exchangeability, data are typically split three ways: one part to train the predictor, one part to fit the transport, and one part to calibrate. This preserves finite-sample validity because the transport is fixed before calibration. However, it is not equivalent to exact conformal prediction (even in one dimension) since the test point is not included when defining the transform; efficiency depends on the quality

of the learned transport, which is statistically hard to estimate in high dimensions (Chewi et al., 2024; Hütter and Rigollet, 2021).

Copula-based multivariate modeling. Another line models the joint distribution of multivariate scores using copulas, after first mapping each coordinate to a uniform scale via empirical marginal distributions (Messoudi et al., 2021; Park et al., 2024). This can produce geometrically adapted multivariate sets. The trade-off is validity: coverage becomes approximate and depends on how well the marginals and copula are estimated. Additional data splitting could be leveraged (Sun and Yu, 2022) to recover the coverage guarantees. Along the same line, recent works Mukama et al. (2024, 2025) describe Copula approaches that preserves the coverage. Similarly, to control joint errors across multiple coordinates, max-rank methods aggregate per-dimension ranks and use a single, more conservative cutoff (Timans et al., 2025). This delivers finite-sample guarantees for family-wise error (equivalently, joint coverage across dimensions), but sets can be larger as a result, and these procedures do not produce predictive distributions.

2 From Prediction Sets to Predictive Distributions: the Univariate Case

When using data-driven predictions in high-stakes situations, it is important not only to make accurate forecasts but also to understand how uncertain these predictions are. When the outcome is a single number (a scalar), this means estimating a range of likely values for the next observation y_{n+1} , given the previous data $D_n = \{(x_1, y_1), \dots, (x_n, y_n)\}$ and a new input x_{n+1} . Conformal prediction sets allow us to construct such ranges without making assumptions on the true data distribution. While a single predicted value gives only one point estimate, conformal prediction sets provide an entire set of plausible values. We can go even further and define an entire predictive distribution, which describes all possible future outcomes for Y_{n+1} and estimate how likely they are. This helps us make better and more informed decisions. In this section, we recall how to obtain conformal prediction sets and predictive distributions from first principles.

2.1 Prediction Sets from the Ground-Truth Distribution

A key tool for constructing prediction set is the Probability Integral Transform (PIT). Let $Z \sim \mathbb{P}$ with a continuous Cumulative Distribution Function $F(z) = \mathbb{P}(Z \leq z)$, then the transformed variable $F(Z)$, so called Probability Integral Transform (PIT), follows a known distribution uniform on $[0, 1]$:

$$F(Z) \sim \text{Uniform}[0, 1].$$

In this uniform space, constructing an uncertainty set is straightforward. For a confidence level $\alpha \in (0, 1)$, any interval $[a, b]$ of length at least $1 - \alpha$ will contain $F(Z)$ with probability larger or equal to $1 - \alpha$. Mapping this interval back to the original space, we obtain the confidence set. More precisely, for a real-valued random variable Z , it is common to construct an interval $[a, b] \subset [0, 1]$, within which it is expected to fall, as a quantile region

$$\mathcal{Q}_\alpha = \{z \in \mathbb{R} : F(z) \in [a, b]\} = Q([a, b]). \quad (1)$$

where $Q = F^{-1}$ is the quantile function. As such, to guarantee a $(1 - \alpha)$ uncertainty region, it suffices to choose a and b (e.g. $a = \alpha/2$ and $b = 1 - \alpha/2$) such that the mass of interval $[a, b]$, measured with the uniform distribution \mathbb{U} , is larger or equal to $1 - \alpha$:

$$\mathbb{P}(Z \in \mathcal{Q}_{1-\alpha}) = \mathbb{U}([a, b]) = b - a \geq 1 - \alpha. \quad (2)$$

However, this result is typically not directly usable, as the ground-truth distribution F of the score is unknown and must be approximated empirically using a finite samples of data.

2.2 Prediction Sets from the Empirical Distribution

The main practical challenge in the construction described earlier is that the true cumulative distribution function F is typically unknown. A natural way to do this is to replace the true CDF F with the empirical distribution given some iid samples z_1, \dots, z_n

$$F_n(z) = F_n(z \mid z_1, \dots, z_n) = \frac{1}{n} \sum_{i=1}^n \mathbf{1}_{z_i \leq z}.$$

However, replacing F with F_n introduces an issue: the empirical probability integral transform no longer produces an exact uniform distribution i.e.

$$F_n(Z) \not\sim \text{Uniform}[0, 1].$$

Only as the number of observations n grows large does the empirical distribution $F_n(Z)$ approach the ideal uniform distribution, and even then, this occurs only asymptotically.

2.2.1 Using Uniform Convergence of Empirical Distribution

Classical statistical results help quantify this approximation error clearly. The Glivenko–Cantelli theorem provides a foundational result here. It states that the empirical distribution F_n converges uniformly to the true distribution F as the sample size increases:

$$\sup_z |F_n(z) - F(z)| \xrightarrow{\text{a.s.}} 0, \quad \text{as } n \rightarrow \infty.$$

Thus, the true prediction set defined by \mathcal{Q}_α can be approximated by a direct plug-in replacement of F by F_n in Equation (1) but this might not preserve the coverage guarantee in Equation (2).

$$\mathcal{Q}_{\alpha,n} = \{z \in \mathbb{R} : F_n(z) \in [a, b]\} = \mathcal{Q}_n([a, b])$$

When the dataset is sufficiently large, this approximate set will typically achieve coverage close to the desired $\mathbb{P}(Z \in \mathcal{Q}_{1-\alpha,n}) \approx 1 - \alpha$. However, this theoretical guarantee applies only in an asymptotic sense; it doesn't tell us exactly how large the dataset must be to have good coverage. To address this practically, we can use the Dvoretzky–Kiefer–Wolfowitz (DKW) (Dvoretzky et al., 1956; Massart, 1990) inequality, a stronger result that explicitly quantifies the approximation error for finite datasets. It states that for any given small error level $\epsilon > 0$,

$$\mathbb{P}\left(\sup_z |F_n(z) - F(z)| > \epsilon\right) \leq 2e^{-2n\epsilon^2}.$$

To build a prediction set using this inequality, we first choose an acceptable probability of error δ . Then we define $\epsilon_n = \sqrt{\frac{\log(2/\delta)}{2n}}$, which ensures that with probability at least $1 - \delta$, $|F_n(z) - F(z)| \leq \epsilon_n$, for all z . Thus, one account for this error by widening our interval

$$\mathcal{Q}_{\delta,1-\alpha,n} = \{z \in \mathbb{R} : F_n(z) \in [a - \epsilon_n, b + \epsilon_n]\},$$

This correction ensures that the resulting empirical prediction set has coverage of at least $1 - \alpha$ with high probability, even for finite sample sizes. These results are especially valuable because they make no assumptions about the shape or nature of the underlying true distribution.

2.2.2 The Conformal Approach

The previous results relied on technical arguments about how quickly the empirical distribution F_n converges to the true distribution F . Conformal prediction (Gammerman et al., 1998; Vovk et al., 2005; Shafer and Vovk, 2008), on the other hand, provides a simpler and more

direct alternative, offering exact uncertainty guarantees for finite samples without relying on convergence rates or asymptotic arguments. Instead of approximating F by F_n and analyzing how quickly this approximation improves as n grows, conformal prediction directly characterizes the distribution of the empirical transform $F_n(Z)$. Under a mild assumption called exchangeability, which means that the ordering of the data points is irrelevant—the distribution of the empirical transform is precisely known, even for finite n .

Lemma 2.1. *If $Z_{n+1} = (Z_1, \dots, Z_n, Z)$ are real-valued exchangeable random variables with no ties, then $F_n(Z)$ follow a discrete uniform measure on a regular grid of $n + 1$ points on $[0, 1]$ i.e.*

$$F_n(Z) \sim \mathbb{U}_{n+1} \left\{ 0, \frac{1}{n}, \frac{2}{n}, \dots, 1 \right\}. \quad (3)$$

That is to say, denoting $\mathbb{P}^{(n+1)}$ as the joint law of Z_{n+1} , it holds

$$\mathbb{P}^{(n+1)}(F_n(Z) \in [a, b]) = \mathbb{U}_{n+1}([a, b]) := \frac{\lfloor nb \rfloor - \lceil na \rceil + 1}{n + 1}. \quad (4)$$

Thus, to build a conformal prediction set, we follow the same intuitive construction as the ideal (ground-truth) case, but now directly in the finite-sample context. Define the UQ set as

$$\mathcal{Q}_{1-\alpha, n} = \{z \in \mathbb{R} : F_n(z) \in [a, b]\}, \quad (5)$$

choosing the endpoints a, b so that the mass of the interval $[a, b]$, measured with the discrete uniform distribution \mathbb{U}_{n+1} , is larger or equal to $1 - \alpha$. By Lemma 2.1, this guarantees the coverage

$$\mathbb{P}(Z \in \mathcal{Q}_{1-\alpha, n}) = \mathbb{U}_{n+1}([a, b]) \geq 1 - \alpha. \quad (6)$$

This approach is fairly straightforward since we did not need to assume that $F_n(Z)$ is close to uniform on $[0, 1]$, nor do we require large sample sizes or convergence rates. The construction precisely mirrors the original ideal case, with an exact finite-sample guarantee, and no further approximations or complicated analyses are required.

In supervised machine learning, we are given a data $\mathcal{D}_n = \{(x_1, y_1), \dots, (x_n, y_n)\}$, a prediction model \hat{y} and a new input X_{n+1} , one can build an uncertainty set for the unobserved output Y_{n+1} by applying the previous process to the observed score functions. The coverage follows directly from the Probability Integral Transform Lemma 2.1; see also (Vovk et al., 2005; Shafer and Vovk, 2008; Angelopoulos et al., 2024).

Proposition 2.1. *Consider $Z_i = S(X_i, Y_i)$ for i in $[n]$ and $Z = S(X_{n+1}, Y_{n+1})$ in Lemma 2.1. The conformal prediction set is defined as*

$$\mathcal{R}_{\alpha, n}(X_{n+1}) = \left\{ y \in \mathcal{Y} : F_n(S(X_{n+1}, y)) \in [a, b] \right\}.$$

For any a and b such that $\mathbb{U}_{n+1}([a, b]) \geq 1 - \alpha$, it satisfies a finite sample coverage guarantee

$$\mathbb{P}(Y_{n+1} \in \mathcal{R}_{\alpha, n}(X_{n+1})) \geq 1 - \alpha.$$

The conformal prediction coverage guarantee in Proposition 2.1 holds for the *unknown* ground-truth distribution of the data \mathbb{P} , does not require quantifying the estimation error $|F_n - F|$, and is applicable to any prediction model \hat{y} as long as it treats the data exchangeably, e.g., a pre-trained model independent of D_n .

We recall here some of the usual description along with few remarks. Leveraging the quantile function $Q_n = F_n^{-1}$, and

- Asymmetric left to right: by setting $a = 0$ and $b = 1 - \alpha$, we have the usual description

$$\mathcal{R}_{\alpha,n}(X_{n+1}) = \{y \in \mathcal{Y} : S(X_{n+1}, y) \leq Q_n(1 - \alpha)\}$$

namely the set of all possible responses whose score rank is smaller or equal to $\lceil(1-\alpha)(n+1)\rceil$ compared to the rankings of previously observed scores. For the absolute value difference score function, the CP set corresponds to $\mathcal{R}_{\alpha,n}(X_{n+1}) = [\hat{y}(X_{n+1}) \pm Q_n(1 - \alpha)]$.

- Center-Outward View: another classical choice is $a = \frac{\alpha}{2}$ and $b = 1 - \frac{\alpha}{2}$. In that case, we have the usual confidence set that corresponds to a range of values that captures the central proportion with $\alpha/2$ of the data lying below $Q(\alpha/2)$ and $\alpha/2$ lying above $Q(1 - \alpha/2)$. Introducing the center-outward distribution of Z as the function $T = 2F - 1$, the probability integral transform $T(Z)$ is uniform in the unit ball $[-1, 1]$. This ensures a symmetric description of $\mathcal{R}_\alpha = T^{-1}(B(0, 1 - \alpha))$ around a central point such as the median $Q(1/2) = T^{-1}(0)$, with the radius of the ball that corresponds to the desired confidence level of uncertainty. Similarly, we have the empirical center-outward distribution $T_n = 2F_n - 1$ and the center-outward view of the conformal prediction set follows as

$$\mathcal{R}_{\alpha,n}(X_{n+1}) = \{y \in \mathcal{Y} : |T_n(S(X_{n+1}, y))| \leq 1 - \alpha\}.$$

- A reader familiar with CP literature would wonder how we are able to use F_n instead of F_{n+1} without breaking exchangeability. It turns out that, in real-valued setting, it holds by definition

$$\begin{aligned} F_{n+1}(Z_{n+1}) &:= F_{n+1}(Z_{n+1} \mid Z_1, \dots, Z_n, Z_{n+1}) \\ &= \frac{n}{n+1}F_n(Z_{n+1}) + \frac{1}{n+1} \\ &= \frac{1}{n+1}\text{Rank}(Z_{n+1}). \end{aligned}$$

So the distribution of $\text{Rank}(Z_{n+1})$ directly provides the distribution of $F_n(Z_{n+1})$. More importantly, the quantile regions of F_{n+1} can be equivalently obtained in term of ones of F_n since for any $\alpha \in (0, 1)$, it holds:

$$F_{n+1}(Z_{n+1}) \leq 1 - \alpha \iff F_n(Z_{n+1}) \leq \frac{(1 - \alpha)(n + 1) - 1}{n}, \quad (7)$$

which essentially recovers the (Angelopoulos et al., 2024, "Replacement Lemma"). However, it is not clear how this equivalence generalizes to higher dimension for which we will rely on the LHS only.

2.3 Predictive Distribution Based on Confidence Distribution

Beyond constructing confidence sets, one may seek a full predictive distribution that quantifies uncertainty over all possible outcomes. We review some of the classical approaches.

2.3.1 Bayesian Predictive Distribution

In the Bayesian framework, inference begins with a prior distribution $p(\theta)$, which encodes initial beliefs about the model parameters θ before observing any data. Given the observed dataset $D_n = \{(x_i, y_i) \text{ for } i \in [n]\}$, the prior is updated via Bayes' theorem to obtain the posterior distribution (Box, 1980; Rubin, 1984; Gelman et al., 1996). It describes the distribution of possible new (unobserved) data conditional on already observed data

$$p(\theta \mid D_n) \propto p(\theta) \prod_{i=1}^n p(y_i \mid x_i, \theta),$$

where $p(y_i | x_i, \theta)$ is the likelihood of the data given the parameters. The Bayesian predictive distribution for a future observation y_{n+1} at a new input x_{n+1} is obtained by averaging the model likelihood over the posterior distribution across all possible values of θ weighted by how likely those parameters θ are given the observations:

$$y \mapsto p(y | x_{n+1}, D_n) = \int_{\Theta} p(y | x_{n+1}, \theta) p(\theta | D_n) d\theta. \quad (8)$$

This integration accounts for both the inherent randomness in the data and the uncertainty in the model parameters. From this predictive distribution, Bayesian prediction intervals also called credible sets $\mathcal{R}_\alpha(x_{n+1})$ for y_{n+1} can be directly constructed by finding the minimum volume region R such that $\int_R p(y \in R | x_{n+1}, D_n) dy \geq 1 - \alpha$. Nevertheless, without additional assumptions (Castillo, 2024), the Bayes credible set does not come with the certificate $\mathbb{P}(Y_{n+1} \in \mathcal{R}_\alpha(x_{n+1})) \geq 1 - \alpha$ for any distribution \mathbb{P} and sample size n .

Beside validity of the credible sets, a notorious difficulty for using Bayesian predictive distribution Equation (8) is that it requires integration over the parameter space Θ . If the latter is high dimensional, the computation might be untractable. However, the Bayesian predictive distribution is doing additional work to incorporate epistemic uncertainties.

2.3.2 Validity Requirement on Predictive Distributions

Previously, we discussed how to construct uncertainty sets. Now, to go beyond sets, our goal is to obtain a complete predictive distribution that itself possesses strong validity guarantees. Ideally, it should be possible to extract valid uncertainty sets directly from such a distribution. This desirable property was not directly achievable by simply using the empirical CDF, as discussed previously. Similarly, Bayesian credible sets do not guarantee this frequentist property without additional assumptions on the prior or in asymptotic regimes.

The Probability Integral Transform (PIT) provides a theoretical foundation for this goal. Recall that for a random variable Z with a continuous CDF $F(z)$, the PIT is the result that $F(Z) \sim \text{Uniform}(0, 1)$. This property is often leveraged to generate samples from F : given a uniform random variable $u \sim \text{Uniform}(0, 1)$, the inverse transform $z = F^{-1}(u)$ produces a sample z from the distribution F . Furthermore, it uniquely identifies the true distribution: if Q is a monotonically increasing function such that $Q(Z) \sim \text{Uniform}(0, 1)$, then necessarily $Q = F$. This uniqueness underscores why satisfying the PIT property is a crucial requirement for any function aiming to be a "valid" representation of the true underlying distribution. In practice, F is unknown. While the empirical CDF, \hat{F}_n , is often used as an estimate, it only satisfies the PIT property asymptotically. While constructing a function that exactly satisfies this property in finite samples is often difficult, it is possible to construct a data-dependent function G_{n+1} that satisfies a (at least a conservative) version of the probability integral transform. This motivates the following definition of predictive distribution from (Shen et al., 2018).

Definition 2.1 (Predictive Distribution Function (Shen et al., 2018)). *Consider a sequence of exchangeable random variable $(X_1, Y_1), \dots, (X_n, Y_n), (X_{n+1}, Y_{n+1})$ where $(X_i, Y_i) \sim \mathbb{P}$. A statistic G is called a predictive distribution function for a new observation Y_{n+1}*

$$\{D_n, (x_{n+1}, y_{n+1})\} \mapsto G(y_{n+1}; x_{n+1}, D_n) \in (0, 1)$$

if it satisfies the following two requirements:

1. For each given data D_n and x_{n+1} , the function $G_{n+1}(y) := G(y; x_{n+1}, D_n)$ is a cumulative distribution function.

2. The random variable $G_{n+1}(Y_{n+1}) := G(Y_{n+1}; X_{n+1}, D_n)$ follows a uniform distribution i.e.

$$\mathbb{P}^{(n+1)}(G_{n+1}(Y_{n+1}) \leq \alpha) = \alpha, \quad \text{for any } \alpha \in (0, 1),$$

Drawing a parallel to the Bayesian approach, which starts by constructing a posterior distribution over the model parameters and then marginalizes it to obtain a predictive distribution, (Shen et al., 2018) construct their predictive distribution by integrating the cumulative distribution function (CDF) of the future outcome over the uncertainty in the model parameters. This uncertainty is captured by a *confidence distribution*. They propose both asymptotic and exact guarantees for the *frequentist coverage properties* of this method. The method proposed by (Shen et al., 2018) for constructing a predictive distribution function, $G(y; x_{n+1}, D_n)$, relies on a distribution over the parameter space for an unknown parameter, θ . A Confidence Distribution, denoted $H(\theta; D_n)$, is a sample-dependent distribution on the parameter space that reflects the uncertainty about θ based on the observed data D_n . The predictive distribution is then formulated as the following integral:

$$G(y; x_{n+1}, D_n) = \int_{\theta \in \Theta} F_{\theta}(y | x_{n+1}) dH(\theta; D_n)$$

In this formula, $F_{\theta}(y | x)$ is the CDF of Y given X , which depends on the parameter θ . This construction effectively averages the possible future distributions over the range of plausible parameter values given by the confidence distribution. The paper establishes theoretical guarantees ensuring that prediction intervals derived from this construction have valid frequentist coverage. Under the condition that the confidence distribution concentrates around the true parameter value as the sample size increases and that $F_{\theta}(\cdot | x)$ is continuous in θ , the method is guaranteed to have *asymptotic coverage*.

However, the approach based on confidence distributions requires knowledge of the parametric form of the ground-truth distribution $F_{\theta}(y | x)$, along with the aforementioned regularity assumptions, to ensure that $\theta \mapsto H(\theta; D_n)$ defines a valid confidence distribution. This requirement can be difficult to satisfy e.g. in the presence of model misspecification and in high-dimensional settings. Also, as with bayesian predictive distribution, the distributions based on confidence distribution also integrate over the high dimensional parameter space which might not be tractable.

2.4 Conformal Predictive Distributions

Remarkably, it is possible to construct a predictive distribution directly from observed data that satisfies a finite-sample version of the probability integral transform, providing strong, distribution-free guarantees. This is achieved by the method of *Conformal Predictive Distributions (CPDs)* (Vovk et al., 2017), which relies only on the assumption of exchangeability of the data points, rather than assuming specific parametric forms of the distribution. It has been studied in some papers (Vovk et al., 2020, 2018; Boström et al., 2021; Johansson et al., 2023). Given scores $\{S_i^y = S(x_i, y_i)\}_{i=1}^n$ and defining the augmented empirical CDF $F_{n+1}(t) = \frac{1}{n+1} \sum_{i=1}^{n+1} \mathbf{1}(S_i^y \leq t)$ for a given candidate y , this yields the (non-randomized) CPD:

$$G_{n+1}(y) = \frac{1}{n+1} \sum_{i=1}^{n+1} \mathbf{1}(S_i^y \leq S_{n+1}^y) = F_{n+1}(S_{n+1}^y | S_1^y, \dots, S_n^y, S_{n+1}^y).$$

Due to the discrete nature of this function (arising from ties in the scores), it only guarantees *conservative* coverage, meaning $\mathbb{P}(G_{n+1}(Y_{n+1}) \leq \alpha) \geq \alpha$.

Randomized CPD for Exact Calibration To achieve exact finite-sample calibration, ties in the conformity scores are broken randomly. This leads to the continuous, randomized CPD:

$$G_{n+1}(y, \tau) = \frac{1}{n+1} \sum_{i=1}^{n+1} \mathbb{1}(S_i^y < S_{n+1}^y) + \frac{\tau}{n+1} \sum_{i=1}^{n+1} \mathbb{1}(S_i^y = S_{n+1}^y),$$

where $\tau \sim \text{Uniform}(0, 1)$ is an auxiliary random variable. This can be expressed more compactly using the empirical CDFs of the scores, and its left-continuous version of the augmented CDF $F_{n+1}^-(t) = \frac{1}{n+1} \sum_{i=1}^{n+1} \mathbb{1}(S_i^y < t)$:

$$G_{n+1}(y, \tau) = (1 - \tau)F_{n+1}^-(S_{n+1}^y) + \tau F_{n+1}(S_{n+1}^y).$$

Under exchangeability, this randomized CPD is a PIT: when evaluated at the true future observation Y_{n+1} , it is exactly uniformly distributed on $[0, 1]$ (Vovk et al., 2017) (see also Lemma 6.1):

$$G_{n+1}(Y_{n+1}, \tau) \sim \text{Uniform}(0, 1).$$

This holds for any finite sample size and without any assumptions on the underlying data-generating distribution. From the exactly-calibrated distribution G_{n+1} , we can derive prediction sets with guaranteed coverage. For a desired confidence level $1 - \alpha$, a valid prediction set is:

$$\Gamma_{1-\alpha}(x_{n+1}) = \{y \in \mathbb{R} : G_{n+1}(y, \tau) \in [\alpha/2, 1 - \alpha/2]\}.$$

As a direct consequence of the exact uniformity of $G_{n+1}(Y_{n+1}, \tau)$, this conformal prediction set has guaranteed marginal coverage:

$$\mathbb{P}(Y_{n+1} \in \Gamma_{1-\alpha}(x_{n+1})) = 1 - \alpha.$$

Choice of the Score Function and Connection to Hypothesis Testing

An insightful perspective is that the mapping $y \mapsto F_n(S(X_{n+1}, y))$ acts as a p-value function for testing the hypothesis: $H_0 : Y_{n+1} = y$ vs $H_1 : Y_{n+1} \neq y$. In fact, the conformal prediction set is exactly the collection of hypotheses y that are not rejected. Building on this, the conformal predictive distribution consists of arranging these individual p-values into a proper cumulative distribution function, ensuring it is monotonically increasing and that evaluating it at the true Y_{n+1} results in a uniformly distributed random variable. However, it is important to emphasize that not every conformity score function S will result in a proper predictive distribution. To ensure that the resulting conformal predictive distribution is valid, the conformity score must satisfy these monotonicity and limit conditions to ensure the conformal predictive distribution constructed from it is valid (Vovk et al., 2017):

- The difference in scores $S_{n+1}^y - S_i^y$ is a monotonically increasing function of $y \in \mathbb{R}$.
- The limits at infinity hold: $\lim_{y \rightarrow -\infty} (S_{n+1}^y - S_i^y) = -\infty$, $\lim_{y \rightarrow +\infty} (S_{n+1}^y - S_i^y) = +\infty$.

The reason is easy to see. By the assumptions, for each index $i \leq n$, the difference $d_i(y) = S_{n+1}^y - S_i^y$ is strictly increasing as a function of y . As $y \rightarrow -\infty$, $d_i(y) \rightarrow -\infty$, and as $y \rightarrow +\infty$, $d_i(y) \rightarrow +\infty$. This means that as we increase y , the set of indices where $S_i^y < S_{n+1}^y$ can only increase, and the set of indices with equality can only shift from equal to strictly less, but not in the reverse direction. As a result, $G_{n+1}(y)$ which counts how many conformity scores are strictly less than the test score, is non-decreasing in y .

3 Multivariate Outputs and Vector-Valued Scores

It is important to highlight that, so far, both Conformal Predictive Distributions and their underlying constructions rely entirely on *real-valued* score functions. In other words, each conformity score S_i^y is a single real number, and the key comparison step $S_i^y \leq S_{n+1}^y$ is only meaningful when the scores can be totally ordered. This total ordering is essential: it is what makes it possible to define cumulative distribution functions, ensure monotonicity, and build valid prediction intervals in a simple and principled way. However, this approach does not directly extend to the multivariate setting, where the label y , and consequently the conformity score S_i^y , becomes a vector in \mathbb{R}^d . In higher dimensions, there is no natural or canonical way to order vectors, so the fundamental comparison $S_i^y \leq S_{n+1}^y$ no longer makes sense. As a result, the core building blocks that enable CPDs in the scalar case, counting, ranking, and defining step functions, cannot be directly applied when scores or labels are multidimensional. Because of this, we cannot currently define conformal prediction sets or predictive distributions with finite-sample guarantees in a straightforward way when using vector-valued scores. The entire framework, as it stands, fundamentally depends on the univariate nature of S_i^y .

3.1 Examples of Vector-Valued Score Function

Model Aggregation / Stacking A natural way to quantify predictive uncertainty when several models are available is to view each model as an "expert" and measure their agreement on the same input. Consider d predictors and define the vector-valued score function

$$s(x, y) = \left[y - \hat{y}_1(x), \dots, y - \hat{y}_d(x) \right] \in \mathbb{R}^d.$$

In this example, the output $y \in \mathbb{R}$ is univariate while the conformity function itself $s(x, y) \in \mathbb{R}^d$ is vector-valued. Similar examples have recently been considered in the classification cases in (Tawachi and Laufer-Goldshtein, 2025). For this setting, classical conformal prediction approaches in Section 2 directly operating on vector-valued score function are not developed yet.

Multi-output Setting When using a multivariate score function $S(x, y) \in \mathbb{R}^q$, the standard univariate conformal prediction approach cannot be applied directly, as it relies on the total order of the real line to define a cumulative distribution function. In the multivariate setting, a natural score should measure the alignment between predictions and ground truth. In classification tasks, each instance belongs to a class $c_i \in \{1, \dots, q\}$ or a categorical label (e.g., {cat, dog}), which we encode as a one-hot vector $y_i \in \{0, 1\}^q$ — for example, $y_i = (1, 0)$ if the image is a cat and $y_i = (0, 1)$ if it is a dog. The model produces logits $z_i \in \mathbb{R}^q$, and the predicted probabilities are obtained via the softmax transformation $\hat{y}_i = \text{softmax}(z_i)$. The alignment between true and predicted labels is measured using the multinomial cross-entropy

$$L_{\text{CE}}(y, \hat{y}) = - \sum_{i=1}^n \sum_{k=1}^q y_{ik} \log \hat{y}_{ik} \text{ and } \nabla_{z_i} \ell(y_i, z_i) = \hat{y}_i - y_i,$$

so a natural vector-valued conformity score is the residual $S(x_i, y_i) := y_i - \hat{y}_i = -\nabla_{z_i} \ell(y_i, z_i)$, which directly encodes how far the predicted probability mass is from the true class indicator.

Another example is in multitask regression, each instance has a continuous target vector $y_i \in \mathbb{R}^q$, where each component corresponds to one of q regression tasks. The model outputs $\hat{y}_i \in \mathbb{R}^q$ as its prediction. The alignment is typically measured by the quadratic loss

$$L_{\text{Quad}}(y, \hat{y}) = \frac{1}{2} \sum_{i=1}^n \|\hat{y}_i - y_i\|_2^2 \text{ and } \nabla_{\hat{y}_i} \ell(y_i, \hat{y}_i) = \hat{y}_i - y_i,$$

leading again to the residual $S(x_i, y_i) := y_i - \hat{y}_i = -\nabla_{\hat{y}_i} \ell(y_i, \hat{y}_i)$.

In both cases, the residual $S(x, y)$ shares the same structure $\hat{y} - y = \nabla_2 L(y, \hat{y}) \in \mathbb{R}^q$, serving as a principled vector-valued conformity score that are particularly suitable for multivariate conformal prediction. These terms naturally appears in generalized linear models McCullagh (2019) or when learning with Fenchel-Young losses (Blondel et al., 2020). As in the previous section, it remains unclear how to conformalize a vector-valued score function.

Vector-Based Approach An initial approach for handling a vector score $s(x, y)$ is to collapse it to a scalar via a norm, for instance, by using its ℓ_2 norm so that classical CP directly applies. However, this discards crucial geometric information. For example, the ℓ_2 norm is rotationally symmetric and cannot distinguish between qualitatively different types of errors, such as a shared model bias (e.g., $[+2, +2]$) and a pure disagreement (e.g., $[+2, -2]$), treating them as identical and then leads to loss of directional semantics. We are also left with a single degree of freedom. The norm provides only a single threshold, preventing fine-grained control over different error types. One cannot, for instance, be lenient on shared bias while being strict on disagreement. A more structured approach using linear maps can partially address this by rotating the score space to decouple error directions (e.g., consensus vs. disagreement), but this is still limited to correcting for linear or elliptical geometries. To handle arbitrary non-linear features of the residual distribution like skewness or curvature, a fully general, non-linear approach is required. This motivates using a transport map T to straighten out the residual distribution by pushing it to a simpler reference distribution, where acceptance regions can be defined. Learning joint dependence with Copulas could also be a good solution. For any of these methods, a critical question remains: how do we select the threshold(s) to ensure a valid $(1 - \alpha)$ coverage guarantee without making assumptions about the ground-truth distribution?

3.2 Multivariate Quantile Region Based on Optimal Transport

In one-dimensional statistics, a point’s rank is determined by the fraction of data that lie below it. It is a distribution-free quantity as no matter what the underlying distribution looks like, the rank of a value z in the sample only depends on how many observations are smaller than or equal to z . However, this clarity vanishes in higher dimensions, where there is no natural way to line up points from smallest to largest. A naive way to define ranks in multiple dimensions might be to measure how far each point is from the origin and then rank them by that distance. But this breaks down if the distribution of the data is stretched or skewed in certain directions. Simply using distances can distort ranks because a big fraction of data might lie in a thin shell, or a small fraction might be spread out in another direction. In short, these raw distances cannot deliver ranks that are distribution-free. Instead of measuring distance in the original data space (where shapes and correlations can vary) optimal transport approach maps the entire data distribution onto a simple and known reference distribution, often chosen as the uniform distribution on a unit ball or cube. This map is found by minimizing the total transport cost, typically measured by squared Euclidean distance. Now the key benefit is that once the data are mapped to a uniform ball, the radial shells in that ball each contain the same fraction of the probability mass. As a result, you can rank a point by its radius in the reference space, effectively capturing how much of the data distribution lies inside that radius. These center-outward ranks then act like univariate ranks-completely distribution-free, because they depend only on proportions of mass, not the specific geometry of the data. These ideas was developed in Chernozhukov et al. (2017); Hallin et al. (2021) developed a framework of center-outward distributions and quantiles, extending the univariate concepts of ranks and quantiles into higher dimensions; which is our main building block for extending conformal prediction framework to vector-valued settings.

Let μ and ν be source and target probability measures on $\Omega \subset \mathbb{R}^d$, both having finite second moments. One can look for a measurable map $T : \Omega \rightarrow \Omega$ that pushes forward μ to ν and minimizes the average transportation cost:

$$T^* \in \operatorname{argmin}_{T_{\#}\mu = \nu} \int_{\Omega} \|z - T(z)\|^2 d\mu(z). \quad (9)$$

Here, the notation $T_{\#}\mu = \nu$ means that T pushes forward the measure μ onto ν , i.e.

$$(T_{\#}\mu)(A) = \mu(T^{-1}(A)), \quad \forall A \subseteq \Omega \text{ measurable.}$$

Equivalently, for every measurable function $f : \Omega \rightarrow \mathbb{R}$,

$$\int_{\Omega} f(y) d\nu(y) = \int_{\Omega} f(T(z)) d\mu(z),$$

so if $Z \sim \mu$, then $T(Z) \sim \nu$ i.e. $T_{\#}\mu = \nu$ simply expresses mass conservation: probability under μ is transported by T to probability under ν .

Brenier's theorem (Brenier, 1991) states that if the source measure μ is absolutely continuous with respect to Lebesgue measure, there exists a unique (up to μ -null sets) solution to Equation (9) that is the gradient of a convex function $\phi : \Omega \rightarrow \mathbb{R}$ such that $T^* = \nabla\phi$. In the one-dimensional case, the cumulative distribution function of a distribution \mathbb{P} is the unique increasing function transporting it to the uniform distribution. This monotonicity property generalizes to higher dimensions through the gradient of a convex function $\nabla\phi$. Thus, one may view the optimal transport map in higher dimensions as a natural analog of the univariate cumulative distribution function: both represent a unique, monotone way to send one probability distribution onto another.

Definition 3.1 (Multivariate Distribution and Rank (Hallin et al., 2021)). *The center-outward distribution of a random variable $Z \sim \mathbb{P}$ is defined via the optimal transport map $T^* = \nabla\phi$ that pushes the distribution \mathbb{P} forward onto the uniform distribution \mathbb{U} supported on the unit ball $B(0, 1) \subset \mathbb{R}^d$, that is $T_{\#}^*\mathbb{P} = \mathbb{U}$. The rank of Z is then defined as the distance from the origin in the transported space: $\operatorname{Rank}(Z) = \|T^*(Z)\|$.*

3.2.1 Quantile Region from the Ground-Truth Distribution

Multivariate quantile regions generalize univariate quantiles, representing regions containing a specified fraction of probability mass. At probability level $r \in (0, 1)$, the quantile region is defined as

$$\mathcal{Q}_r = \{z \in \mathbb{R}^d : \|T^*(z)\| \leq r\} = (T^*)^{-1}(B(0, r)).$$

By definition, the optimal transport map satisfies the marginal (pushforward) constraint. Hence,

$$T_{\#}^*\mathbb{P} = \mathbb{U} \implies \mathbb{P}(Z \in \mathcal{Q}_r) = (T_{\#}^*\mathbb{P})(B(0, r)) = \mathbb{U}(B(0, r)). \quad (10)$$

Thus, it suffices to choose a radius

$$r_{\alpha} := \inf\{r \in [0, 1] : \mathbb{U}(B(0, r)) \geq 1 - \alpha\}$$

so that $\mathbb{P}(Z \in \mathcal{Q}_{r_{\alpha}}) \geq 1 - \alpha$. This choice is *distribution-free*, i.e., it does not depend on \mathbb{P} .

Choice of the Target Distribution Following Hallin et al. (2021), the target distribution $\nu = \mathbb{U}$ is taken to be the *spherical uniform distribution*, which represents a random vector in \mathbb{R}^d obtained by first choosing a direction uniformly on the unit sphere and then selecting a radius uniformly from $[0, 1]$. Because the volume element in spherical coordinates grows as

r^{d-1} , maintaining a uniform distribution in r requires compensating by a factor of $1/r^{d-1}$. The resulting density on $\mathbb{B}(0,1) \setminus \{0\}$ is

$$f(\mathbf{u}) = \frac{\mathbb{1}_{\mathbb{B}(0,1) \setminus \{0\}}(\mathbf{u})}{c_d} \times \frac{1}{\|\mathbf{u}\|^{d-1}}, \quad c_d = \frac{2\pi^{d/2}}{\Gamma(d/2)} = |\mathbb{S}^{d-1}|,$$

where c_d is the surface area of the unit sphere, ensuring that the total probability mass integrates to one. By construction, the radial component $R = \|T^*(Z)\|$ is uniformly distributed on $(0,1)$, so that exact coverage holds with $r_\alpha = 1 - \alpha$, i.e.

$$\mathbb{P}(Z \in \mathcal{Q}_{1-\alpha}) = 1 - \alpha. \quad (11)$$

Hence, this generalizes the construction of the quantile region in the multivariate setting (Section 2.1) using the ground-truth distribution. As in the univariate case, this oracle construction cannot be used in practice, since the ground-truth distribution \mathbb{P} is unknown.

3.2.2 Validity Loss due to Approximations

In practice, the true score distribution is unknown, and we only have access to a finite set of calibration scores, $\{Z_1, \dots, Z_n\}$. Consequently, the continuous optimal transport problem is replaced by its computationally tractable empirical counterpart. This is achieved by transporting the *empirical source measure*, $\mu_n = \frac{1}{n} \sum_{i=1}^n \delta_{Z_i}$, to a *discrete target measure*, $\nu_n = \frac{1}{n} \sum_{j=1}^n \delta_{U_j}$, defined on a fixed set of canonical points $\{U_1, \dots, U_n\}$. The problem of finding the optimal transport plan between these two discrete measures is a classic *assignment problem*. It reduces to finding an optimal permutation $\sigma_n \in \mathfrak{S}_n$ that minimizes the total transportation cost:

$$\sigma_n \in \operatorname{argmin}_{\sigma \in \mathfrak{S}_n} \sum_{i=1}^n \|Z_i - U_{\sigma(i)}\|^2,$$

where \mathfrak{S}_n is the set of all permutations of $\{1, \dots, n\}$.

The solution, σ_n , defines the empirical transport map T_n by assigning each source point to its corresponding target point:

$$T_n(Z_i) := U_{\sigma_n(i)}.$$

By construction, this map perfectly pushes the empirical source measure forward to the target measure, ensuring that $T_{n\#}\mu_n = \nu_n$. This is because the map simply reorders the atoms of μ_n to match the locations of the atoms of ν_n . However, such maps are defined only on the discrete set $\{Z_1, \dots, Z_n\}$, so an out-of-sample extension is required to apply T_n to new test points. Given such an empirical estimator (with extrapolation) T_n of the Brenier map, one defines the approximate quantile region

$$\mathcal{Q}_{1-\alpha,n} := T_n^{-1}(B(0, 1 - \alpha)), \text{ and expect } \mathbb{P}(Z \in \mathcal{Q}_{1-\alpha,n}) \approx 1 - \alpha.$$

Exact coverage as in Equation (11) is not guaranteed unless we can control the approximation error $\|T_n - T^*\|$, which typically requires strong regularity assumptions. This issue arises even in the one-dimensional case and becomes more critical in higher dimensions. Indeed, the empirical transport map suffers from statistical limitations due to the curse of dimensionality (Chewi et al., 2024). In general, practical implementations of OT-based quantile regions must account for approximation errors due to both finite-sample estimation and deviations introduced by regularizations. Plugging in an approximate map $T_{n,\varepsilon}$ involves additional regularity assumptions (compromising the distribution-free guarantee) and unknown universal constants (compromising finite-sample guarantees). Hence, the approximate quantile region may remain invalid even asymptotically.

4 Multivariate Conformal Prediction via Optimal Transport

In this section, we develop a conformal prediction framework for fully vector-valued score functions that relies solely on the probability integral transform (PIT) defined via optimal transport. This yields a natural multivariate extension of classical conformal prediction without introducing any intermediate learning step or additional data splitting. We also analyze coverage when the exact transport map is replaced by a regularized or empirical approximation.

We consider the *discrete* transport map

$$T_{n+1} : (Z_i)_{i \in [n+1]} \mapsto (U_i)_{i \in [n+1]},$$

obtained by solving the optimal assignment problem:

$$T_{n+1} \in \operatorname{argmin}_{T \in \mathcal{T}} \sum_{i=1}^{n+1} \|Z_i - T(Z_i)\|^2, \quad (12)$$

where \mathcal{T} is the set of bijections between the observed sample $(Z_i)_{i \in [n+1]}$ and the target grid $(U_i)_{i \in [n+1]}$. Following Hallin et al. (2021), we construct the target distribution $\nu_{n+1} = \mathbb{U}_{n+1}$ as a discrete approximation of the spherical uniform law. It is defined such that $n+1 = n_R n_S + n_o$, where:

- n_o points are placed at the origin;
- n_S unit vectors $\mathbf{u}_1, \dots, \mathbf{u}_{n_S}$ are uniformly distributed on the unit sphere;
- n_R radii are regularly spaced as $\left\{ \frac{1}{n_R}, \frac{2}{n_R}, \dots, 1 \right\}$.

The grid discretizes the sphere into concentric shells, each containing n_S equally spaced points along directions determined by the unit vectors. The discrete spherical uniform distribution assigns equal mass to each grid point, with $n_o/(n+1)$ mass at the origin and $1/(n+1)$ on the remaining points. This ensures isotropic sampling over $[0, 1]$ in the radial direction.

By construction of the discrete transport map T_{n+1} , we have

$$\|T_{n+1}(Z_{n+1})\| \text{ has empirical distribution } \mathbb{U}_{n+1} \text{ supported on } \left\{ 0, \frac{1}{n_R}, \frac{2}{n_R}, \dots, 1 \right\}, \quad (13)$$

providing a discrete analogue of the probability integral transform. However, the transport map T_{n+1} is fitted on both Z_1, \dots, Z_n and the unknown test point Z_{n+1} . As in the univariate conformal setting, the conformal construction replaces Z_{n+1} by all possible candidate values $Z \in \mathbb{R}^d$, recomputing the map for each candidate, which is computationally demanding.

4.1 Conformalized Quantile Region

4.1.1 Augmented Transport Map

Let $Z_1, \dots, Z_n \in \mathbb{R}^d$ be fixed source points and $U_1, \dots, U_{n+1} \in \mathbb{R}^d$ be fixed target points. For a query point $Z \in \mathbb{R}^d$, we define the empirical source measure and the target measure as

$$\mu_Z = \frac{1}{n+1} \left(\sum_{i=1}^n \delta_{Z_i} + \delta_Z \right) \quad \text{and} \quad \nu_{n+1} = \frac{1}{n+1} \sum_{j=1}^{n+1} \delta_{U_j}.$$

An optimal transport plan between μ_Z and ν corresponds to a permutation $\sigma_Z \in \mathfrak{S}_{n+1}$ that solves

$$\sigma_Z \in \operatorname{argmin}_{\sigma \in \mathfrak{S}_{n+1}} \left(\sum_{i=1}^n \|Z_i - U_{\sigma(i)}\|^2 + \|Z - U_{\sigma(n+1)}\|^2 \right).$$

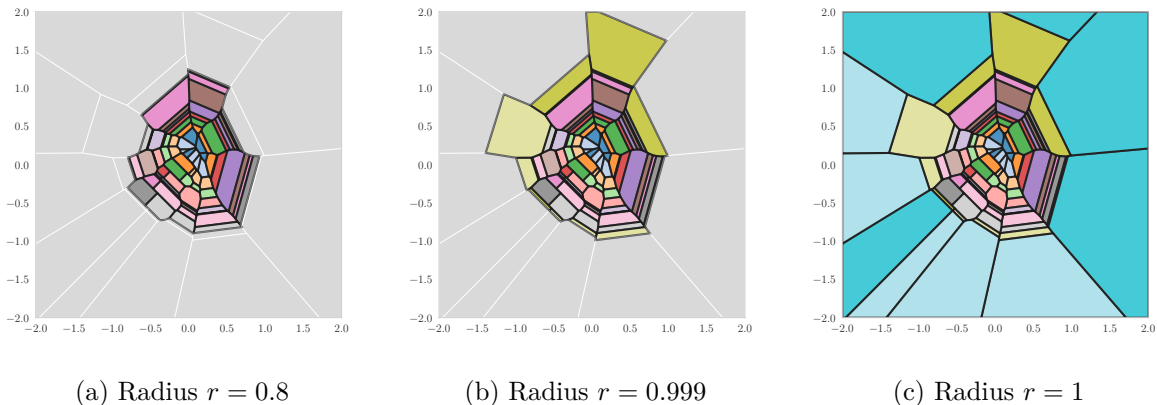


Figure 1: Illustration of the active cells Ω_r for various radius. It is bounded whenever $r < 1$ and might be unbounded otherwise. In uncertainty quantification, $r = r_\alpha$ is the radius corresponding to a level of confidence $1 - \alpha$ and is strictly smaller than one for every $\alpha \in [0, 1)$.

This permutation induces a full transport map T_{n+1}^Z on the augmented sample (Z_1, \dots, Z_n, Z) by setting $T_{n+1}^Z(Z_i) = U_{\sigma_Z(i)}$ for $i \in \{1, \dots, n\}$ and $T_{n+1}^Z(Z) = U_{\sigma_Z(n+1)}$. Our primary object of interest is the assignment map $\psi : \mathbb{R}^d \rightarrow \{U_1, \dots, U_{n+1}\}$ for the query point itself, defined as

$$\psi(Z) := T_{n+1}^Z(Z) = U_{\sigma_Z(n+1)}.$$

Note that the entire map T_{n+1}^Z depends on the location of Z , since it alters the source measure μ_Z . As a result, $\psi(Z)$ is not computed from a single, fixed transport map but from a family of maps indexed by Z . Although the pushforward identity $T_{n+1}^Z \# \mu_Z = \nu_{n+1}$ holds exactly for the empirical measures, it is not immediately clear why this construction should yield valid statistical guarantees that we could obtain if $T_{n+1}^Z \# \mathbb{P} = \nu_{n+1}$. In general, empirical validity does not imply population validity; that is, a procedure guaranteed to cover a high fraction of the specific points used to build the map does not automatically provide coverage for a new point drawn from the true underlying law \mathbb{P} . This is the fundamental gap that conformal prediction framework bridges by assuming exchangeability of the data.

4.1.2 Coverage Guarantee

Using this, we define the augmented empirical quantile region as

$$\mathcal{Q}_r := \left\{ z \in \mathbb{R}^d : \|T_{n+1}^z(z)\| := \|U_{\sigma_z(n+1)}\| \leq r \right\},$$

where $r \in [0, 1]$ is a threshold radius to be selected according to Proposition 4.1 in order to achieve a user prescribed coverage level. We propose below an algorithm to compute the *finite* collection of transport map needed and illustrate the quantile region obtained in Figure 2 and Figure 3.

Crucially, this approach differs from using a transport map trained only on the first n data points: the inclusion of all possible candidate $z \in \mathbb{R}^d$ in the transport computation ensures that the quantile region reflects the uncertainty associated with a new test point. In contrast, regions based on T_n fitted without augmentation may not provide valid coverage guarantees, as they ignore the effect of the test point on the induced transport geometry. We show how to select a data-driven radius $r_{\alpha, n+1}$ such that the conformal prediction region satisfies the exact finite-sample coverage guarantee.

Proposition 4.1 (Coverage of the Conformalized Quantile Region). *Let Z_1, \dots, Z_n, Z_{n+1} be exchangeable. Given n discrete sample points following the discrete spherical uniform distribution*

with n_S is the number of such directions, n_R is the number of radius, and n_o is the number of copies of the origin. Defining the radius as

$$r_{\alpha, n+1} = \frac{j_\alpha}{n_R} \text{ where } j_\alpha = \left\lceil \frac{(n+1)(1-\alpha) - n_o}{n_S} \right\rceil,$$

it holds:

$$\mathbb{P}(Z_{n+1} \in \mathcal{Q}_{r_{\alpha, n+1}}) \geq 1 - \alpha$$

4.2 Multivariate Prediction Set

As in the one dimensional case, we can consider supervised machine learning setting where one observes both features X_i and their corresponding label Y_i for $i \in [n]$. Given a new input X_{n+1} , the corresponding conformal prediction set is obtained as:

$$\mathcal{R}_{\alpha, n+1}(X_{n+1}) = \left\{ y \in \mathcal{Y} : \|T_{n+1}^y(S(X_{n+1}, y))\| \leq r_{\alpha, n+1} \right\}, \quad (14)$$

where we recall that for any candidate $y \in \mathcal{Y}$, T_{n+1}^y is an optimal transport map pushing the source points $(S(X_1, Y_1), \dots, S(X_n, Y_n), S(X_{n+1}, y))$ to the target points $(U_i)_{i \in [n+1]}$.

Proposition 4.2. *The conformal prediction set is defined as*

$$\mathcal{R}_{\alpha, n+1}(X_{n+1}) = \{y \in \mathcal{Y} : \|T_{n+1}^y(S(X_{n+1}, y))\| \leq r_{\alpha, n+1}\}$$

It satisfies a distribution-free finite sample coverage guarantee

$$\mathbb{P}(Y_{n+1} \in \mathcal{R}_{\alpha, n+1}(X_{n+1})) \geq 1 - \alpha. \quad (15)$$

4.3 A Tractable Algorithm via Polyhedral Partitions

While conceptually appealing, the previous construction faces major computational limitations. For every candidate $y \in \mathbb{R}^d$, the empirical transport map T_{n+1}^y must be recomputed to include the test score $S(X_{n+1}, y)$ along with the calibration scores. Since \mathbb{R}^d contains infinitely many candidates, this implies an unbounded number of transport map computations, making the procedure intractable even for moderate sample sizes. A natural workaround is to restrict attention to a finite subset $\text{Grid} \subset \mathbb{R}^d$, but this introduces two challenges. First, the conformal coverage guarantee no longer applies exactly, since $\mathcal{R}_\alpha(X_{n+1}) \cap \text{Grid}$ may fail to contain Y_{n+1} with probability $1 - \alpha$. Second, computing the prediction set still requires fitting a separate transport map for each point in the grid, leading to significant computational cost if the grid is large. In high dimensions, the number of grid points needed for accurate approximation can grow exponentially in d , further exacerbating the problem. Similar problems appears when computing full conformal prediction set (i.e. refitting the model itself for every test candidates) for one dimensional regression setting; see (Chen et al., 2016; Johnstone and Ndiaye, 2022; Ndiaye and Takeuchi, 2019; Ndiaye, 2022; Martinez et al., 2023).

In the next section, we introduce an algorithm that completes the prediction set construction in finitely many steps by exploiting the regularity structure of discrete transport maps.

Proposition 4.3. *Let $Z_1, \dots, Z_n \in \mathbb{R}^d$ be fixed source points and $U_1, \dots, U_{n+1} \in \mathbb{R}^d$ fixed target points. Let C_k denote the optimal transport cost from $\{Z_1, \dots, Z_n\}$ to $\{U_j\}_{j \neq k}$:*

$$C_k := \min_{\sigma} \sum_{i=1}^n \|Z_i - U_{\sigma(i)}\|^2, \text{ where } \sigma : [n] \mapsto [n+1] \setminus \{k\} \text{ is a bijection.}$$

Then, for any query point $Z \in \mathbb{R}^d$, define the cost function:

$$f_k(Z) := \|Z - U_k\|^2 + C_k.$$

Let $k^*(Z) := \operatorname{argmin}_k f_k(Z)$ be the index that minimizes this cost. Define the assignment map:

$$\psi(Z) := U_{k^*(Z)}.$$

Let σ_Z^* be the permutation defined by:

- $\sigma_Z^*(n+1) := k^*(Z)$,
- and σ_Z^* restricted to $[n]$ is the optimal permutation matching $\{Z_i\}_{i \in [n]}$ to $\{U_j\}_{j \neq k^*(Z)}$.

Then the full assignment defined by σ_Z^* is an optimal transport map from μ_Z to ν_{n+1} .

The assignment map $\psi(Z)$ selects the target point U_j minimizing $f_j(Z)$ where each constant C_j is precomputed from the fixed sources Z_1, \dots, Z_n . A key observation is that each cost function $f_j(Z)$ is quadratic, and the difference between two such functions is always affine and then the region where f_j is minimal, denoted

$$\mathcal{R}_j = \{Z \in \mathbb{R}^d : f_j(Z) \leq f_k(Z) \forall k \neq j\},$$

is thus a polyhedron defined by finitely many half-spaces, each corresponding to a pairwise comparison with another target point. Since there are only n other targets $k \neq j$, only a finite number of linear inequalities are needed to fully describe each region \mathcal{R}_j . The collection $\{\mathcal{R}_j\}_{j=1}^{n+1}$ forms a partition of \mathbb{R}^d . Each region corresponds to a fixed transport assignment: on \mathcal{R}_j , the query point Z is matched to U_j i.e. $\psi(Z) = U_j$. These regions are entirely determined by the positions of the targets and the precomputed costs C_j . Once computed, this partition is fixed and independent of Z .

Proposition 4.4 (Polyhedral Partition). *The assignment map $\psi : \mathbb{R}^d \rightarrow \{U_1, \dots, U_{n+1}\}$ defined in Proposition 4.3 induces a partition of the source space: $\mathbb{R}^d = \bigcup_{j=1}^{n+1} \mathcal{R}_j$, where each region $\mathcal{R}_j := \{Z \in \mathbb{R}^d : \psi(Z) = U_j\}$ is a convex polyhedron described by*

$$\mathcal{R}_j = \left\{ Z \in \mathbb{R}^d : \langle Z, U_k - U_j \rangle \leq \beta_{j,k} \text{ for all } k \neq j \right\},$$

where $\beta_{j,k} := \frac{1}{2}(\|U_k\|^2 - \|U_j\|^2 + C_k - C_j)$.

To represent regions \mathcal{R}_j as a collection of half-spaces, the decision region attached to label j is

$$\mathcal{R}_j = \{Z \in \mathbb{R}^d : A_j Z \leq b_j\}$$

by stacking the corresponding row vectors and constants gives

$$A_j = \begin{pmatrix} (U_{k_1} - U_j)^T \\ (U_{k_2} - U_j)^T \\ \vdots \\ (U_{k_n} - U_j)^T \end{pmatrix} \in \mathbb{R}^{n \times d} \text{ and } b_j = \begin{pmatrix} \beta_{j,k_1} \\ \beta_{j,k_2} \\ \vdots \\ \beta_{j,k_n} \end{pmatrix} \in \mathbb{R}^n$$

Alternatively, membership in region \mathcal{R}_j can be efficiently checked and plotted numerically via:

$$\mathcal{R}_j = \{Z \in \mathbb{R}^d : L(Z) \leq 0\} \text{ where } L(Z) = \max_{k \neq j} \langle Z, U_k - U_j \rangle - \beta_{j,k}.$$

4.4 Boundness and Computation of the Quantile Region

We are interested in evaluating the sublevel set

$$\Omega_r = \{Z \in \mathbb{R}^d : |\psi(Z)| \leq r\},$$

which captures all query points whose assigned target under ψ lies within a ball of radius r centered at the origin. Since the assignment map $\psi(Z)$ is constant on each region \mathcal{R}_j , the condition $|\psi(Z)| \leq r$ is equivalent to $|U_j| \leq r$ for the index j such that $Z \in \mathcal{R}_j$. As such, we define the active variables and we obtain the decomposition

$$\Omega_r = \bigcup_{j \in I_r} \mathcal{R}_j, \text{ where } I_r := \{j \in [n+1] : |U_j| \leq r\}.$$

As each region \mathcal{R}_j is a convex polyhedron defined by affine inequalities, the set Ω_r is a union of convex polyhedra easily computable once the regions \mathcal{R}_j and the target norms $|U_j|$ are known. The importance of this result is that we do not need to test infinitely many candidates to characterize the quantile region. As such, for the shift $Z = y - \hat{y}(x)$, we have

$$\Omega_r(x) = \hat{y}(x) + \Omega_r = \hat{y}(x) + \psi^{-1}(B(0, r)),$$

where the second equality holds since the map ψ is piecewise constant, its inverse ψ^{-1} is set-valued and corresponds to a polyhedral partition of the input space. For each target point U_j , the preimage $\psi^{-1}(U_j)$ is the region $\mathcal{R}_j \subset \mathbb{R}^d$ consisting of all inputs Z assigned to U_j . Hence, for any subset $S \subset \mathbb{R}^d$, the inverse image is given by $\psi^{-1}(S) = \bigcup_{j: U_j \in S} \mathcal{R}_j$. Thus

$$\psi^{-1}(B(0, r)) = \bigcup_{j \in I_r} \psi^{-1}(U_j) = \bigcup_{j \in I_r} \mathcal{R}_j = \Omega_r.$$

The following result shows that the region Ω_r is bounded. The rationale is that an unbounded polyhedron \mathcal{R}_j would imply that the corresponding point U_j must be on the boundary of the convex hull of all target points. Since active regions for $r < 1$ correspond to interior points, they must be bounded. We provide illustration in Figure 1.

Proposition 4.5 (Boundness of the Conformal Quantile Region). *For any radius $r < 1$ and target points selected from spherical uniform distribution, the active cells Ω_r is bounded.*

4.5 Multivariate Predictive Distribution

Definition 4.1 (Multivariate Predictive Distribution Map). *Let $\{(X_i, Y_i)\}_{i=1}^{n+1}$ be exchangeable with common law \mathbb{P} on $\mathcal{X} \times \mathbb{R}^d$. Fix the spherical uniform distribution as reference law \mathbb{U} . Given data $D_n = \{(X_i, Y_i)\}_{i=1}^n$ and a new input x_{n+1} , a statistic*

$$G : \{D_n, (x_{n+1}, y)\} \mapsto G(y; x_{n+1}, D_n) \in \mathbb{R}^d$$

is called a multivariate predictive distribution map if, for each (x_{n+1}, D_n) , the function

$$G_{n+1}(y) := G(y; x_{n+1}, D_n) : \mathbb{R}^d \mapsto B(0, 1)$$

satisfies:

1. (Center-outward structure) G_{n+1} is a center-outward distribution map:
2. (Probability-integral transform) The multivariate PIT holds

$$G_{n+1}(Y_{n+1}) \sim \mathbb{U} \quad \text{under the joint law of } (X_1, Y_1), \dots, (X_{n+1}, Y_{n+1}).$$

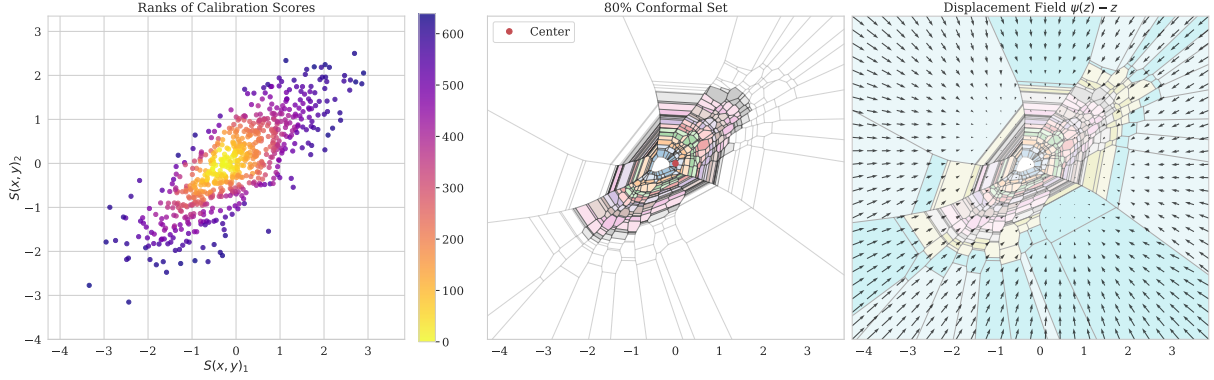


Figure 2: **Anisotropic Gaussian Distribution.** Illustration of the Multivariate conformalized quantile region when the conformity scores \mathbf{Z} are generated from a mean-centered Gaussian distribution. The prediction model is the null model $\hat{y}(\mathbf{x}) = \mathbf{0}$ and the covariance structure is set as $\mathbf{Y} \sim \mathcal{N}(\mathbf{0}, \Sigma)$, where $\Sigma = \begin{pmatrix} 1 & 0.8 \\ 0.8 & 1 \end{pmatrix}$.

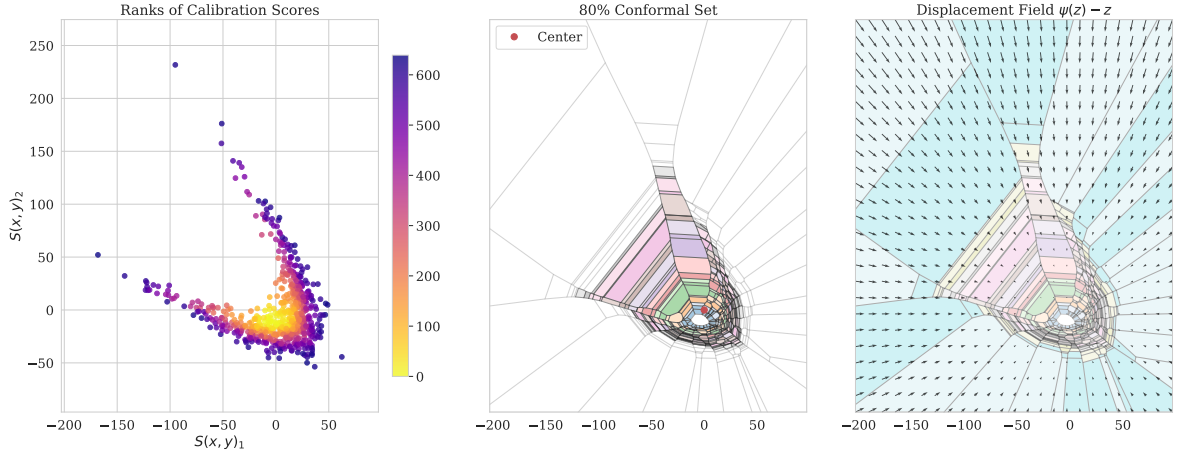


Figure 3: **A skewed distribution.** We illustrate geometric adaptivity when the scores $\mathbf{Z} = (Z_1, Z_2)^\top$ are generated from a nonlinear transformation of standard normal variables. The scores follow $\mathbf{Y} = R(X_{\text{err}}, Y_{\text{err}})^\top$, where $Y_{\text{err}} = 15Z_2 + 24(Z_1^2 - 1)$ and R is a 45° rotation matrix.

To extend conformal predictive distributions (CPD) to the multivariate setting, we adopt an optimal transport-based generalization. Interestingly, it does not require integration over the parameter space compared to previous approaches.

Definition 4.2 (Vector-Valued Conformal Predictive Distribution System). *We define*

$$\mathcal{T}_{n+1} : y \in \mathbb{R}^d \mapsto T_{n+1}^y(S(X_{n+1}, y)) \in \mathbb{R}^d,$$

where, for each $y \in \mathbb{R}^d$, T_{n+1}^y denotes the optimal transport map sending the empirical distribution of $(S(X_1, Y_1), \dots, S(X_n, Y_n), S(X_{n+1}, y))$ to the empirical distribution of the points $(U_i)_{i=1}^{n+1}$.

As in the one dimensional setting, validity is obtained by characterizing the target distribution when $y = Y_{n+1}$ following the PIT. The following proposition does so when $Z_i = S(X_i, Y_i)$ for $i \in [n+1]$. To exactly match the continuous distribution \mathbb{U} , an additional randomization step will be needed. We describe it later, using semi-discrete optimal transport.

Theorem 4.1. *Let T_{n+1} be the optimal assignment between $\{Z_i\}$ and $\{U_j\}$. Then,*

$$\mathbb{P}^{(n+1)}(T_{n+1}(Z_{n+1}) \in A) = \mathbb{U}_{n+1}(A).$$

We remind that the assignment map $\psi : \mathbb{R}^d \rightarrow \{U_1, \dots, U_{n+1}\}$ is defined as $\psi(Z) := U_{\sigma_Z(n+1)}$, which assigns the target point matched to Z under the optimal plan. Note that σ_Z depends on the location of Z itself, since it alters the empirical source distribution μ_Z . As a result, $Z \mapsto \psi(Z)$ is not computed from a fixed map but instead from a family of transport maps indexed by Z . This dependency requires a slightly additional care: although each individual optimal transport plan is cyclically monotone, the map $Z \mapsto \psi(Z)$ aggregates assignments from infinitely many such problems.

Proposition 4.6. *Let $Z^{(1)}, \dots, Z^{(m)} \in \mathbb{R}^d$ be a finite set of query points. For each $l \in \{1, \dots, m\}$, let $\sigma^{(l)} \in S_{n+1}$ denote the permutation that solves the optimal transport problem from $\mu_{Z^{(l)}}$ to \mathbb{U} and so $\psi(Z^{(l)}) := U_{\sigma^{(l)}(n+1)}$, i.e., the target assigned to the query point $Z^{(l)}$. Then, the set of pairs $\{(Z^{(l)}, \psi(Z^{(l)}))\}_{l=1}^m$ is cyclically monotone i.e. for $Z^{(m+1)} := Z^{(1)}$, it holds*

$$\sum_{l=1}^m \|Z^{(l)} - \psi(Z^{(l)})\|^2 \leq \sum_{l=1}^m \|Z^{(l)} - \psi(Z^{(l+1)})\|^2,$$

Furthermore, the map $Z \mapsto \psi(Z) = U_{\sigma_Z(n+1)}$ is monotone.

Unfortunately, monotonicity is not generally preserved under composition, so we look for a simple sufficient conditions under which the vector-valued conformal predictive transformation

$$y \mapsto \mathcal{T}_{n+1}(y) = T_{n+1}^y(S(X_{n+1}, y)) = \psi(S(X_{n+1}, y))$$

remains monotone in y . In the special case of the residual score $S(x, y) = y - \hat{y}(x)$, we have

$$S(X_{n+1}, y) - S(X_{n+1}, y') = y - y'.$$

Thus, by monotonicity of ψ , it holds

$$\langle \mathcal{T}_{n+1}(y) - \mathcal{T}_{n+1}(y'), y - y' \rangle = \langle \psi(S(X_{n+1}, y)) - \psi(S(X_{n+1}, y')), S(X_{n+1}, y) - S(X_{n+1}, y') \rangle \geq 0.$$

Proposition 4.7. *If $S(x, y) = y - \hat{y}(x)$, then $y \mapsto \mathcal{T}_{n+1}(y)$ is a monotone operator.*

Characterizing necessary and sufficient condition on the score function in order to obtain a monotone appears to be quite difficult for us and we leave as an open problem. Indeed, even for general affine score functions with positive semi-definite matrix i.e. $S(x, y) = Ay + b$ with $A \succeq 0$, the previous argument only yields

$$\langle \mathcal{T}_{n+1}(y) - \mathcal{T}_{n+1}(y'), y - y' \rangle_{A^{1/2}} = \langle \mathcal{T}_{n+1}(y) - \mathcal{T}_{n+1}(y'), A(y - y') \rangle \geq 0,$$

i.e., monotonicity in the metric induced by the matrix A . Euclidean monotonicity need not hold unless A has special structure (e.g., $A = \lambda I_d$).

It is also worth noting that the scalarized version $y \mapsto \|T_{n+1}^y(S(X_{n+1}, y))\|$ is not necessarily monotone. The norm discards directional information and keeps only the magnitude. It might still be an interesting map but its regularity property need to be properly studied in future work.

Remark 4.1 (*Full Conformal Predictive Distribution System*). *We highlight that here we consider the setting of **split** conformal prediction where the prediction model $x \mapsto \hat{y}(x)$ was trained on a dataset D_{train} independent of $D_n = \{(x_i, y_i) \text{ for } i \in [n]\}$. If instead we consider the **full** CP setting where the model \hat{y} is recomputed on the augmented dataset $D_n \cup \{x_{n+1}, y\}$ for every $y \in \mathbb{R}^d$, we could not provide a general monotonicity result.*

5 Randomized Conformal Predictive Distribution and Generalization of the Dempster-Hill Procedure

5.1 One Dimensional Dempster-Hill

Dempster (1963) method of *direct probabilities* is a classical nonparametric predictive distribution for the next observation Y_{n+1} when you have IID real-valued data with no covariates. It assigns equal probability mass $1/(n+1)$ to each of the $n+1$ gaps formed by the sorted sample (including the two tails). It proceeds as follow: sort the observed sample $y_{(1)} \leq \dots \leq y_{(n)}$ and define $y_{(0)} = -\infty, y_{(n+1)} = \infty$. Then, the predictive Dempster-Hill distribution $Q_{n+1}(y)$ is

$$Q_{n+1}(y) = \begin{cases} \left[\frac{i}{n+1}, \frac{i+1}{n+1}\right] & \text{if } y \in (y_{(i)}, y_{(i+1)}) \\ \left[\frac{i-1}{n+1}, \frac{i+1}{n+1}\right] & \text{if } y = y_{(i)} \end{cases} \quad \text{for } i \in \{0, \dots, n\},$$

i.e., Y_{n+1} is equally likely to fall in any open interval between successive order statistics. At ties you get an interval of CDF values; and randomization picks a point inside it. Under IID/exchangeability, this yields exact finite-sample validity: the randomized CDF value $Q_{n+1}(Y_{n+1})$ is Uniform(0,1). Equivalently, a $(1 - \alpha)$ prediction set is obtained by taking the union of the middle $(1 - \alpha)$ fraction of gaps e.g select the central interval $[y_{(k)}, y_{(n+1-k)}]$. Since

$$\mathbb{P}\left(Y_{n+1} \in [y_{(k)}, y_{(n+1-k)}]\right) = \frac{(n+1-k) - k}{n+1} \geq 1 - \alpha \text{ for } k = \lfloor \alpha(n+1)/2 \rfloor.$$

Interestingly, Vovk et al. (2017) highlighted that the Dempster-Hill procedure is exactly the conformal predictive system. Given a conformity measure $A : \mathbb{R}^{n+1} \rightarrow \mathbb{R}$, the conformal transducer outputs, for a candidate label y and a tie-breaker $\tau \sim \text{Unif}(0, 1)$, is defined as

$$Q_{n+1}(y, \tau) = \frac{\#\{i \leq [n+1] : \alpha_i(y) < \alpha_{n+1}(y)\}}{n+1} + \tau \times \frac{\#\{i \leq [n+1] : \alpha_i(y) = \alpha_{n+1}(y)\}}{n+1},$$

where every score equals the corresponding value: $\alpha_i(y) = y_i$ for $i \leq n$ and $\alpha_{n+1}(y) = y$. This is the standard conformal predictive system (CPS) construction in (Vovk et al., 2017) that outputs an interval version

$$Q_{n+1}(y) = [Q_{n+1}(y, 0), Q_{n+1}(y, 1)].$$

- If $y \in (y_{(i)}, y_{(i+1)})$ (no ties), then exactly i of the y_j are below y and none equals y . Hence

$$Q_{n+1}(y, \tau) = \frac{i}{n+1} \quad \text{for all } \tau \in [0, 1],$$

so the interval version (with a thickness of $1/(n+1)$) is

$$Q_{n+1}(y) = [Q_{n+1}(y, 0), Q_{n+1}(y, 1)] = \left[\frac{i}{n+1}, \frac{i+1}{n+1}\right]$$

- If $y = y_{(i)}$ and there are ties at that value among $\{y_1, \dots, y_n, y\}$, then let the tied block be $y_{(i')} = \dots = y_{(i'')} = y$ with $i' \leq i \leq i''$. Then $\#\{y_j < y\} = i' - 1$ and $\#\{y_j = y\} = (i'' - i' + 1) + 1$ to account for the test value y . Therefore

$$Q_{n+1}(y, \tau) = \frac{i' - 1}{n+1} + \tau \cdot \frac{i'' - i' + 2}{n+1},$$

giving the interval version

$$Q_{n+1}(y) = [Q_{n+1}(y, 0), Q_{n+1}(y, 1)] = \left[\frac{i' - 1}{n+1}, \frac{i'' + 1}{n+1}\right].$$

Putting these cases together, and simplifying the number of ties to $y = y_{(i)}$ so that value appears only once i.e. $i' = i'' = i$, which yields exactly the Dempster–Hill rule:

$$Q_{n+1}(y) = \begin{cases} \left[\frac{i}{n+1}, \frac{i+1}{n+1} \right], & y \in (y_{(i)}, y_{(i+1)}), \\ \left[\frac{i-1}{n+1}, \frac{i+1}{n+1} \right], & y = y_{(i)}, \end{cases}$$

i.e., the next observation is equally likely to fall in any gap between successive order statistics, with uniform randomization inside ties. As such, the Dempster–Hill procedure is indeed a conformal predictive system.

Optimal Transport View of Dempster-Hill Procedure

In the one-dimensional Dempster-Hill or conformal predictive setting, we have IID data y_1, \dots, y_{n+1} . The predictive CDF $Q_{n+1}(y, \tau)$ assigns equal probability $1/(n+1)$ to each of the $n+1$ intervals formed by the ordered sample. For a candidate y , the randomized CDF value

$$Q_{n+1}(y, \tau) = \frac{\#\{y_i < y\}}{n+1} + \tau \frac{\#\{y_i = y\}}{n+1}, \quad \tau \sim \text{Unif}(0, 1),$$

is uniformly distributed in $(0, 1)$ under exchangeability. If the distribution is discontinuous, one cannot reach all coverage level for all $\alpha \in (0, 1)$ which leads to conservative approach. Randomization replaces the jump of the discrete CDF at ties by a continuous layer, producing exact finite-sample validity:

$$Q_{n+1}(Y_{n+1}, \tau) \sim \text{Unif}(0, 1).$$

Thus, Dempster-Hill can be interpreted as a discrete randomized transport from μ_{n+1} to the uniform target on $(0, 1)$. This same principle extends naturally to semi-discrete optimal transport. Let the source be discrete, $\mu = \sum_i a_i \delta_{\zeta_i}$, and the target continuous, \mathbb{U} with CDF $F_{\mathbb{U}}$. Each source atom ζ_i carries mass a_i and is mapped to a target *cell*

$$I_i = [F_{\mathbb{U}}^{-1}(s_{i-1}), F_{\mathbb{U}}^{-1}(s_i)], \quad s_i = \sum_{j \leq i} a_j.$$

Randomization inside each I_i ensures that the transported sample is distributed according to \mathbb{U} :

$$T(\zeta_i, \tau_i) = F_{\mathbb{U}}^{-1}((1 - \tau_i)s_{i-1} + \tau_i s_i), \quad \tau_i \sim \text{Unif}(0, 1).$$

When all $a_i = 1/(n+1)$ and $\mathbb{U} = \text{Unif}(0, 1)$, this reduces exactly to the Dempster-Hill rule i.e. it sets equal mass $1/(n+1)$ per gap and do a uniform randomization inside that gap.

If several sample values coincide, say $y_{(i')} = \dots = y_{(i'')} = y$, their individual intervals merge into one larger quantile block $I_{[i', i'']} = \left[\frac{i'-1}{n+1}, \frac{i''}{n+1} \right]$. The randomized map becomes

$$T(y, \tau) = (1 - \tau) \frac{i' - 1}{n+1} + \tau \frac{i''}{n+1} \sim \text{Unif} \left(\frac{i' - 1}{n+1}, \frac{i''}{n+1} \right) \text{ for } \tau \sim \text{Unif}(0, 1),$$

or, for a general continuous target \mathbb{U} with CDF $F_{\mathbb{U}}$,

$$T(y, \tau) = F_{\mathbb{U}}^{-1} \left((1 - \tau) \frac{i' - 1}{n+1} + \tau \frac{i''}{n+1} \right).$$

Hence, ties correspond to merged quantile cells in the target domain and then randomization inside the merged interval restores exact calibration.

5.2 Multivariate Dempster-Hill via Semi-Discrete Optimal Transport

The classical Dempster-Hill predictive rule can be viewed as a one-dimensional optimal transport (OT) construction: each sample point y_i carries equal mass $1/(n+1)$ and is mapped to an interval of length $1/(n+1)$ in $(0, 1)$, so that randomizing uniformly within that interval yields a $\text{Unif}(0, 1)$ variable. In multiple dimensions, the same structure holds geometrically. The discrete Dempster-Hill "gaps" become Laguerre cells in the target space. To obtain a *continuous* predictive distribution, we embed this discrete assignment into a semi-discrete OT framework between the empirical source μ_{n+1} and a continuous target \mathbb{U} (e.g., the spherical-uniform law).

Following the formulation in (Lévy et al., 2025), introduce weights $w = (w_j)_{j \in [n+1]}$ and define the Laguerre cells as

$$A_j(w) = \left\{ y : \|y - U_j\|^2 + w_j \leq \|y - U_k\|^2 + w_k, \forall k \right\}.$$

The optimal weights w^* solve the semi-discrete dual problem

$$K(w) = \frac{1}{n+1} \sum_{j=1}^{n+1} w_j + \int_Y \min_j (\|y - U_j\|^2 + w_j) d\mathbb{U}(y), \quad \frac{\partial K}{\partial w_j} = \frac{1}{n+1} - \mathbb{U}(A_j(w)),$$

By first order optimality condition, the optimal weights w^* enforce equal-mass cells,

$$\mathbb{U}(A_j(w^*)) = \frac{1}{n+1}, \quad j = 1, \dots, n+1.$$

These convex regions $\{A_j(w^*)\}$ form a tessellation of the target space. Note that this entire stage is independent of the source data $\{Z_i\}$. It only depends on the target measure \mathbb{U} and the chosen sites U_j . The optimal assignment σ^* send point Z_i to the cell $A_j(w^*)$ that is "closest" to it. More precisely, we can define a Per-cell expected costs. For any $z \in \mathbb{R}^d$ and any index $k \in [n+1]$, the expected squared cost of sending z to the cell A_k with conditional law \mathbb{U}_k is

$$\bar{c}(z, k) = \int_{A_k} \|z - u\|^2 d\mathbb{U}_k(u) \text{ where } \mathbb{U}_k := \mathbb{U}(\cdot | A_k). \quad (16)$$

We then obtain a discrete assignment problem matching the source points and the target cells:

$$\sigma^* = \operatorname{argmin}_{\sigma \in \mathfrak{S}_{n+1}} \sum_{i=1}^{n+1} \bar{c}(z, \sigma(i))$$

Now to generalize the one-dimensional quantile intervals of Dempster-Hill, we can look at the semi-discrete optimal plan is

$$\pi^* = \frac{1}{n+1} \sum_{i=1}^{n+1} \delta_{Z_i} \otimes \mathbb{U}(\cdot | A_{\sigma^*(i)}(w^*)),$$

meaning that each Z_i is mapped uniformly within its assigned cell $A_{\sigma^*(i)}(w^*)$. The corresponding randomized map is

$$\tilde{T}_{n+1}(Z_i, \tau) \sim \mathbb{U}(\cdot | A_{\sigma^*(i)}(w^*)),$$

where τ is auxiliary randomness used to sample uniformly inside the cell. By construction, $\tilde{T}_{n+1}(Z_{n+1}, \tau) \sim \mathbb{U}$, so the transformed point has the exact target law (as a multivariate PIT).

Theorem 5.1 (Randomized Semi-Discrete PIT). *Let (Z_1, \dots, Z_{n+1}) be exchangeable random variables in \mathbb{R}^d with joint law $\mathbb{P}^{(n+1)}$. Fix a continuous target distribution \mathbb{U} and an equal-mass*

Laguerre partition $\{A_k\}_{k \in [n+1]}$ satisfying $\mathbb{U}(A_k) = \frac{1}{n+1}$. Let σ^* be the semi-discrete optimal assignment and define the randomized map

$$\tilde{T}_{n+1}(Z_i, \tau_i) \sim \mathbb{U}_{\sigma^*(i)} \quad \text{independently in } i,$$

where the auxiliary seeds τ_i are i.i.d. and independent of the data. Then, for any subset B ,

$$\mathbb{P}^{(n+1)}(\tilde{T}_{n+1}(Z_{n+1}, \tau) \in B) = \mathbb{U}(B).$$

In 1D, randomization fills the discrete jumps of the empirical CDF. In higher dimensions, it fills each Laguerre cell with continuous uniform draws. In both cases, randomization converts a discrete mapping into a continuous, measure-preserving transport. When \mathbb{U} is the spherical-uniform distribution, the image of Z_{n+1} under \tilde{T}_{n+1} is uniformly distributed on the unit ball, with radius $\|\tilde{T}_{n+1}(Z_{n+1}, \tau)\| \sim \text{Unif}(0, 1)$. The Dempster-Hill randomization and the semi-discrete OT framework are two views of the same principle: Randomization \iff continuous sampling within equal-mass OT cells. In one dimension, these cells are quantile intervals; in multiple dimensions, they are convex Laguerre regions $A_j(w^*)$. In both settings, the resulting randomized map yields exact uniformization of the predictive transform: $\tilde{T}(Z_{n+1}, \tau) \sim \mathbb{U}$.

5.3 Semi-discrete Assignment Stream and Randomized Transport

We now give the exact analogue of the discrete "assignment stream" for the semi-discrete setting where the source is discrete and the target is the continuous spherical law on the unit ball. We call it stream because we connect (Z_1, \dots, Z_n, Z) to fixed target but the $(n+1)$ th source point Z changes continuously in \mathbb{R}^d and require a transport map for each of them. The key replacement is that each target point U_k is substituted by its Laguerre (power) cell A_k in the target, and the pointwise cost $\|Z - U_k\|^2$ is replaced by the *expected* cost of transporting to the conditional target law in cell A_k . Let us denote the first and second conditional moments of \mathbb{U}_k

$$m_k := \int u d\mathbb{U}_k(u) = \mathbb{E}[U \mid U \in A_k], \quad s_k := \int \|u\|^2 d\mathbb{U}_k(u) = \mathbb{E}[\|U\|^2 \mid U \in A_k].$$

The following proposition shows how to extend the polyhedral partition algorithm.

Proposition 5.1 (Semi-discrete assignment stream). *Let Z_1, \dots, Z_n be fixed and let $\{A_k\}_{k=1}^{n+1}$ be Laguerre cells with $\mathbb{U}(A_k) = \frac{1}{n+1}$. Define the $n \times (n+1)$ cost matrix $\bar{c}_{i,k} := \bar{c}(Z_i, k)$ using (16).*

For each k , let

$$C_k := \min_{\sigma} \sum_{i=1}^n \bar{c}_{i, \sigma(i)}, \quad \text{where } \sigma : [n] \mapsto [n+1] \setminus \{k\} \text{ is a bijection} \quad (17)$$

be the optimal n -to- n assignment cost when column k is removed. For a query $Z \in \mathbb{R}^d$, define

$$f_k(Z) := \bar{c}(Z, k) + C_k, \quad k^*(Z) := \underset{k \in [n+1]}{\operatorname{argmin}} f_k(Z). \quad (18)$$

Let σ_Z^ be any bijection on $[n+1]$ such that $\sigma_Z^*(n+1) = k^*(Z)$ and the restriction $\sigma_Z^*|_{[n]}$ attains the minimum in (17) with $k = k^*(Z)$. Then:*

1. Optimal augmented semi-discrete assignment. σ_Z^* solves the augmented semi-discrete assignment

$$\min_{\tilde{\sigma}} \sum_{i=1}^n \bar{c}(Z_i, \tilde{\sigma}(i)) + \bar{c}(Z, \tilde{\sigma}(n+1)), \quad \text{where } \tilde{\sigma} : [n+1] \rightarrow [n+1] \text{ is a bijection.} \quad (19)$$

2. Randomized transport is optimal. Define the randomized map

$$\tilde{T}_{n+1}^Z(Z, \tau) \sim \mathbb{U}_{\sigma_Z^*(n+1)} = \mathbb{U}(\cdot \mid A_{k^*(Z)}), \quad \tilde{T}_{n+1}^Z(Z_i, \tau_i) \sim \mathbb{U}_{\sigma_Z^*(i)} = \mathbb{U}(\cdot \mid A_{\sigma_Z^*(i)}), i \leq n,$$

with $\tau, \tau_1, \dots, \tau_n$ i.i.d. auxiliary randomness independent of the data. Then the coupling

$$\pi_Z^* = \frac{1}{n+1} \sum_{i=1}^{n+1} \delta_{\zeta_i} \otimes \mathbb{U}_{\sigma_Z^*(i)}, \quad \zeta_{n+1} := Z, \zeta_i := Z_i \quad (i \leq n),$$

is an optimal semi-discrete transport plan from the augmented source μ_Z to the continuous target \mathbb{U} .

3. Polyhedral partition of the source. For each k , the decision region

$$\mathcal{R}_k := \{Z \in \mathbb{R}^d : f_k(Z) \leq f_\ell(Z) \forall \ell\}$$

is a convex polyhedron. In particular, for every ℓ ,

$$f_k(Z) - f_\ell(Z) = -2\langle Z, m_k - m_\ell \rangle + (s_k - s_\ell) + (C_k - C_\ell),$$

and hence \mathcal{R}_k is an affine half-space.

If each cell A_k degenerates to a single point U_k (i.e. $\mathbb{U}_k = \delta_{U_k}$), then $m_k = U_k$ and $s_k = \|U_k\|^2$, so $\bar{c}(z, k) = \|z - U_k\|^2$. Thus, proposition 5.1 reduces to the discrete result in proposition 4.3.

Once a maximizer of the semi-discrete dual has been computed so that $\mathbb{U}(A_k) = 1/(n+1)$, the randomized map \tilde{T}_{n+1}^Z implements an exact multivariate probability integral transform: for Z_{n+1} exchangeable with $\{Z_i\}$ and τ independent, $\tilde{T}_{n+1}^{Z_{n+1}}(Z_{n+1}, \tau) \sim \mathbb{U}$. Pulling back any target set of \mathbb{U} -mass $1 - \alpha$ yields exact finite-sample coverage $1 - \alpha$.

The summaries (m_k, s_k) depend only on \mathbb{U} and the cells A_k . The constants C_k are computed by solving $n+1$ linear assignment problems on the matrix $(\bar{c}_{i,k})$ with column k removed. After this precomputation, evaluating $\psi(Z) = A_{k^*(Z)}$ is $O(n)$ in k and constructing $\tilde{T}_{n+1}^Z(Z, \tau)$ is a single conditional draw in $A_{k^*(Z)}$. In-fine, we have finite catalogue of streaming transport maps i.e there exist bijections $\sigma^{(1)}, \dots, \sigma^{(n+1)}$ on $[n]$ (one per removed column) such that the optimal augmented plan for any query Z uses one of the *finitely many* transport maps

$$\left\{ \pi_Z^{(k)} := \frac{1}{n+1} \sum_{i=1}^n \delta_{Z_i} \otimes \mathbb{U}_{\sigma^{(k)}(i)} + \frac{1}{n+1} \delta_Z \otimes \mathbb{U}_k \right\}_{k \in [n+1]},$$

chosen according to $k = k^*(Z)$. Equivalently, the source space \mathbb{R}^d is partitioned into at most $n+1$ convex polyhedra $\{\mathcal{R}_k\}$, and on each \mathcal{R}_k the entire optimal transport plan (including the randomized representation) is determined by the single precomputed assignment $\sigma^{(k)}$. The semi-discrete structure first partitions the *target* via power cells $\{A_k\}$ of equal \mathbb{U} -mass; the streaming formulation then induces a *source* partition $\{\mathcal{R}_k\}$.

5.3.1 Monotonicity of the Semi-discrete Assignment Stream

Let us define the semi-discrete assignment map to the *cell* and to its *barycenter* by

$$\psi_{\text{sd}}(Z) := A_{k^*(Z)}, \quad \phi_{\text{sd}}(Z) := m_{k^*(Z)}.$$

Proposition 5.2 (Cyclical monotonicity in expected cost). *Let $Z^{(1)}, \dots, Z^{(m)} \in \mathbb{R}^d$ be a finite set of query points. For each l , let $k_l := k^*(Z^{(l)})$ and choose a permutation $\sigma^{(l)}$ on $[n+1]$ such that $\sigma^{(l)}(n+1) = k_l$ and $\sigma^{(l)}|_{[n]}$ achieves C_{k_l} in (17). Define $\sigma^{(m+1)} := \sigma^{(1)}$.*

(i) *For $U^{(l)} \sim \mathbb{U}(\cdot | A_{k_l})$ and $U^{(l+1)} \sim \mathbb{U}(\cdot | A_{k_{l+1}})$, independent of the data, one has*

$$\sum_{l=1}^m \mathbb{E} \|Z^{(l)} - U^{(l)}\|^2 \leq \sum_{l=1}^m \mathbb{E} \|Z^{(l)} - U^{(l+1)}\|^2.$$

(ii) (Pairwise monotonicity of the barycentric map.) *In particular, for $m = 2$,*

$$\langle Z^{(1)} - Z^{(2)}, \phi_{\text{sd}}(Z^{(1)}) - \phi_{\text{sd}}(Z^{(2)}) \rangle \geq 0.$$

Consequently, the set of pairs $\{(Z^{(l)}, \phi_{\text{sd}}(Z^{(l)}))\}_{l=1}^m$ is cyclically monotone (hence ϕ_{sd} is the subgradient of a convex function on each region where $k^(\cdot)$ is constant). Moreover, the graph of the randomized mapping $Z \mapsto \tilde{T}_{n+1}(Z, \tau) \sim \mathbb{U}(\cdot | \psi_{\text{sd}}(Z))$ is cyclically monotone.*

The proof mirrors the discrete case verbatim once pointwise costs $\|Z - U_k\|^2$ are replaced by the expected cell costs $\bar{c}(Z, k)$.

5.3.2 Boundedness and Computation of the Semi-Discrete Quantile Region

Recall the semi-discrete assignment map to cells

$$\psi_{\text{sd}} : \mathbb{R}^d \mapsto \{A_1, \dots, A_{n+1}\}, \quad \psi_{\text{sd}}(Z) := A_{k^*(Z)},$$

where the decision regions $\mathcal{R}_k := \{Z \in \mathbb{R}^d : k^*(Z) = k\}$ form a polyhedral partition of \mathbb{R}^d (Proposition 5.1). Each region \mathcal{R}_k of the source is paired with one target cell A_k of the partition of the unit ball, so that every query point $Z \in \mathcal{R}_k$ is transported (randomly) inside A_k .

Definition. We define the semi-discrete quantile region at level $r \in (0, 1]$ as the set of query points whose entire image cell lies within the ball of radius r :

$$\Omega_r^{\text{sd}} = \{Z \in \mathbb{R}^d : \|\tilde{T}_{n+1}^Z(Z, \tau)\| \leq r \text{ a.s. for all } \tau\}.$$

Since ψ_{sd} is constant on each \mathcal{R}_k , this is equivalent to requiring $A_{k^*(Z)} \subseteq B(0, r)$. Define the active index set

$$I_r := \{k \in [n+1] : A_k \subseteq B(0, r)\},$$

so that

$$\Omega_r^{\text{sd}} = \bigcup_{k \in I_r} \mathcal{R}_k.$$

As each \mathcal{R}_k is a convex polyhedron described by affine inequalities, Ω_r^{sd} is a finite union of convex polyhedra. It is therefore easy to compute once the regions $\{\mathcal{R}_k\}$ and cells $\{A_k\}$ (or inclusion certificates $A_k \subseteq B(0, r)$) are known. As in the discrete case, this eliminates the need to scan infinitely many candidates $Z \in \mathbb{R}^d$. For a shift $Z = y - \hat{y}(x)$, one expresses the quantile region as

$$\Omega_r^{\text{sd}}(x) = \hat{y}(x) + \Omega_r^{\text{sd}} = \hat{y}(x) + \psi_{\text{sd}}^{-1}(\{A_k : A_k \subseteq B(0, r)\}),$$

where $\psi_{\text{sd}}^{-1}(A_k) = \mathcal{R}_k$ denotes the preimage of the k -th target cell.

Proposition 5.3 (Boundedness of the semi-discrete quantile region). *For any radius $r < 1$, the uncertainty set Ω_r^{sd} is bounded.*

The argument mirrors the discrete case, with target points U_j replaced by cell barycenters m_k . The supporting-hyperplane argument extends because the Laguerre partition covers all boundary directions of the unit ball.

6 Discussion and Future Work

This work introduces a framework for extending conformal prediction to multivariate settings using optimal transport. While we have established the core theoretical properties and provided a tractable algorithm, our results also highlight several important limitations and open up exciting avenues for future research.

Tractability, Complexity, and Potential Approximations

A central contribution of this paper is a tractable algorithm for constructing the exact OT-based conformal set by pre-computing a polyhedral partition of the score space. This reduces a problem over an infinite domain to a finite one. It is important, however, to be precise about the nature of this tractability. The pre-computation stage requires solving $n + 1$ separate $n \times n$ assignment problems to find the costs $\{C_k\}$, leading to a total computational complexity of $\mathcal{O}(n^4)$ using standard solvers. While this is a significant theoretical advance over a brute-force approach, this complexity can be prohibitive for applications with large calibration sets. A natural path to reduce this computational burden is to approximate the pre-computation of the C_k constants. For instance, one could:

- Replace the exact $\mathcal{O}(n^3)$ assignment problem solver with a much faster, entropically regularized one, such as the Sinkhorn algorithm Sinkhorn (1964); Cuturi (2013) or auction algorithm Bertsekas (1988). This could reduce the total complexity to approximately $\mathcal{O}(n^3)$.
- Restrict the regularity of the transport map itself, for example, by assuming it belongs to a simpler parametric family like linear maps $T(x) = Ax + b$. Closed form formulas are available and significantly drop the computational complexity.

However, these approximations can fundamentally alter the theoretical guarantee of our framework. They would yield approximate costs \hat{C}_k and, consequently, an approximate polyhedral partition. The assignment of a test point would no longer be exact. The consequences of such approximations on the final calibration are not known; we leave it for future work.

Scope and Validity of the Multivariate CPD

We presented the first construction of a multivariate Conformal Predictive Distribution (CPD) with finite-sample calibration guarantees. A cornerstone of a valid predictive distribution is its monotonicity (or cyclical monotonicity in \mathbb{R}^d). We provide a formal proof of this property under the important and common setting of residual scores (i.e., $S(x, y) = y - \hat{y}(x)$) within a split-conformal framework. However, we must emphasize that this proof does not yet extend to more general score functions. As we note in our analysis, characterizing the necessary and sufficient conditions on the score function to ensure the cyclical monotonicity of the resulting map remains a challenging open problem. Furthermore, our monotonicity results are currently limited to the split-CP setting; they do not apply to the full CP setting where the model itself is retrained.

References

- Angelopoulos, A. N., Barber, R. F., and Bates, S. (2024). Theoretical foundations of conformal prediction. *arXiv preprint arXiv:2411.11824*.
- Bertsekas, D. P. (1988). The auction algorithm: A distributed relaxation method for the assignment problem. *Annals of operations research*, 14(1):105–123.
- Blondel, M., Martins, A. F., and Niculae, V. (2020). Learning with fenchel-young losses. *Journal of Machine Learning Research*, 21(35):1–69.

- Boström, H., Johansson, U., and Löfström, T. (2021). Mondrian conformal predictive distributions. In *Conformal and Probabilistic Prediction and Applications*, pages 24–38. PMLR.
- Box, G. E. (1980). Sampling and bayes’ inference in scientific modelling and robustness. *Journal of the Royal Statistical Society Series A: Statistics in Society*, 143(4):383–404.
- Braun, S., Aolaritei, L., Jordan, M. I., and Bach, F. (2025). Minimum volume conformal sets for multivariate regression. *arXiv preprint arXiv:2503.19068*.
- Brenier, Y. (1991). Polar factorization and monotone rearrangement of vector-valued functions. *Communications on Pure and Applied Mathematics*, 44(4).
- Castillo, I. (2024). Bayesian nonparametric statistics, st-flour lecture notes. *arXiv preprint arXiv:2402.16422*.
- Chen, W., Wang, Z., Ha, W., and Barber, R. F. (2016). Trimmed conformal prediction for high-dimensional models. *arXiv preprint arXiv:1611.09933*.
- Chernozhukov, V., Galichon, A., Hallin, M., and Henry, M. (2017). Monge–Kantorovich depth, quantiles, ranks and signs. *The Annals of Statistics*, 45(1):223 – 256.
- Chewi, S., Niles-Weed, J., and Rigollet, P. (2024). Statistical optimal transport. *arXiv preprint arXiv:2407.18163*.
- Cuturi, M. (2013). Sinkhorn distances: Lightspeed computation of optimal transport. In *Advances in neural information processing systems*, pages 2292–2300.
- Dawid, A. P. (1984). Present position and potential developments: Some personal views statistical theory the prequential approach. *Journal of the Royal Statistical Society: Series A (General)*, 147(2):278–290.
- Dempster, A. P. (1963). On direct probabilities. *Journal of the Royal Statistical Society: Series B (Methodological)*, 25(1):100–110.
- Dheur, V., Fontana, M., Estievenart, Y., Desobry, N., and Taieb, S. B. (2025). Multi-output conformal regression: A unified comparative study with new conformity scores.
- Diebold, F. X., Gunther, T. A., and Tay, A. (1997). Evaluating density forecasts.
- Dvoretzky, A., Kiefer, J., and Wolfowitz, J. (1956). Asymptotic minimax character of the sample distribution function and of the classical multinomial estimator. *The Annals of Mathematical Statistics*, pages 642–669.
- Fong, E. and Holmes, C. C. (2021). Conformal bayesian computation. *Advances in Neural Information Processing Systems*, 34:18268–18279.
- Gamerman, A., Vovk, V., and Vapnik, V. (1998). Learning by transduction.
- Gelman, A., Meng, X.-L., and Stern, H. (1996). Posterior predictive assessment of model fitness via realized discrepancies. *Statistica sinica*, pages 733–760.
- Gneiting, T., Balabdaoui, F., and Raftery, A. E. (2007). Probabilistic forecasts, calibration and sharpness. *Journal of the Royal Statistical Society Series B: Statistical Methodology*, 69(2):243–268.
- Hallin, M., del Barrio, E., Cuesta-Albertos, J., and Matrán, C. (2021). Distribution and quantile functions, ranks and signs in dimension d: A measure transportation approach. *The Annals of Statistics*, 49(2):1139 – 1165.

- Hamill, T. M. (2001). Interpretation of rank histograms for verifying ensemble forecasts. *Monthly Weather Review*, 129(3):550–560.
- Hullman, J., Wu, Y., Xie, D., Guo, Z., and Gelman, A. (2025). Conformal prediction and human decision making. *arXiv preprint arXiv:2503.11709*.
- Hütter, J.-C. and Rigollet, P. (2021). Minimax estimation of smooth optimal transport maps.
- Johansson, U., Löfström, T., and Boström, H. (2023). Conformal predictive distribution trees. *Annals of Mathematics and Artificial Intelligence*, pages 1–14.
- Johnstone, C. and Cox, B. (2021). Conformal uncertainty sets for robust optimization. In Carlsson, L., Luo, Z., Cherubin, G., and An Nguyen, K., editors, *Proceedings of the Tenth Symposium on Conformal and Probabilistic Prediction and Applications*, volume 152 of *Proceedings of Machine Learning Research*, pages 72–90. PMLR.
- Johnstone, C. and Ndiaye, E. (2022). Exact and approximate conformal inference in multiple dimensions. *arXiv preprint arXiv:2210.17405*.
- Kiyani, S., Pappas, G., Roth, A., and Hassani, H. (2025). Decision theoretic foundations for conformal prediction: Optimal uncertainty quantification for risk-averse agents. *arXiv preprint arXiv:2502.02561*.
- Klein, M., Bethune, L., Ndiaye, E., and Cuturi, M. (2025). Multivariate conformal prediction using optimal transport. *arXiv preprint arXiv:2502.03609*.
- Lanngren, S., Toremark, M., and Szabadváry, J. H. (2025). Conformal predictive decision making: A comparative study with bayesian and point-predictive methods. *Proceedings of Machine Learning Research*, 266:1–26.
- Lawless, J. F. and Fredette, M. (2005). Frequentist prediction intervals and predictive distributions. *Biometrika*, 92(3):529–542.
- Lévy, B., Ray, N., Mérigot, Q., and Leclerc, H. (2025). Large-scale semi-discrete optimal transport with distributed voronoi diagrams. *Journal of Computational Physics*, 542:114374.
- Martinez, J. A., Bhatt, U., Weller, A., and Cherubin, G. (2023). Approximating full conformal prediction at scale via influence functions. In *Proceedings of the AAAI Conference on Artificial Intelligence*, volume 37, pages 6631–6639.
- Massart, P. (1990). The tight constant in the dvoretzky-kiefer-wolfowitz inequality. *The annals of Probability*, pages 1269–1283.
- McCullagh, P. (2019). *Generalized linear models*. Routledge.
- Messoudi, S., Destercke, S., and Rousseau, S. (2021). Copula-based conformal prediction for multi-target regression. *Pattern Recognition*, 120:108101.
- Messoudi, S., Destercke, S., and Rousseau, S. (2022). Ellipsoidal conformal inference for multi-target regression. In *Conformal and Probabilistic Prediction with Applications*, pages 294–306. PMLR.
- Mukama, B. C., Messoudi, S., Destercke, S., and Rousseau, S. (2025). Copula-based conformal prediction for prioritized heterogeneous multi-task learning. *Pattern Recognition*, page 112347.
- Mukama, B. C., Messoudi, S., Rousseau, S., and Destercke, S. (2024). Copula-based conformal prediction for object detection: a more efficient approach. In *13th Symposium on Conformal and Probabilistic Prediction with Applications*, volume 230, pages 140–157.

- Ndiaye, E. (2022). Stable conformal prediction sets. In *International Conference on Machine Learning*, pages 16462–16479. PMLR.
- Ndiaye, E. and Takeuchi, I. (2019). Computing full conformal prediction set with approximate homotopy. *Advances in Neural Information Processing Systems*, 32.
- Park, J. W., Tibshirani, R., and Cho, K. (2024). Semiparametric conformal prediction. *arXiv preprint arXiv:2411.02114*.
- Pion, A. and Vazquez, E. (2025). A bayesian framework for calibrating gaussian process predictive distributions. *Proceedings of Machine Learning Research*, 266:1–3.
- Rubin, D. B. (1984). Bayesianly justifiable and relevant frequency calculations for the applied statistician. *The Annals of Statistics*, pages 1151–1172.
- Shafer, G. and Vovk, V. (2008). A tutorial on conformal prediction. *Journal of Machine Learning Research*.
- Shen, J., Liu, R. Y., and Xie, M.-g. (2018). Prediction with confidence—a general framework for predictive inference. *Journal of Statistical Planning and Inference*, 195:126–140.
- Sinkhorn, R. (1964). A relationship between arbitrary positive matrices and doubly stochastic matrices. *Ann. Math. Statist.*, 35:876–879.
- Sun, S. and Yu, R. (2022). Copula conformal prediction for multi-step time series forecasting. *arXiv preprint arXiv:2212.03281*.
- Tawachi, Y. and Laufer-Goldshtein, B. (2025). Multi-dimensional conformal prediction. In *The Thirteenth International Conference on Learning Representations*.
- Thurin, G., Nadjahi, K., and Boyer, C. (2025). Optimal transport-based conformal prediction.
- Timans, A., Straehle, C.-N., Sakmann, K., Naeseth, C. A., and Nalisnick, E. (2025). Max-rank: Efficient multiple testing for conformal prediction. In *The 28th International Conference on Artificial Intelligence and Statistics*.
- Vovk, V. (2019). Universally consistent conformal predictive distributions. In *conformal and probabilistic prediction and applications*, pages 105–122. PMLR.
- Vovk, V. and Bendtsen, C. (2018). Conformal predictive decision making. In *Conformal and Probabilistic Prediction and Applications*, pages 52–62. PMLR.
- Vovk, V., Gammerman, A., and Shafer, G. (2005). *Algorithmic learning in a random world*. Springer.
- Vovk, V., Nouretdinov, I., Manokhin, V., and Gammerman, A. (2018). Cross-conformal predictive distributions. In *conformal and probabilistic prediction and applications*, pages 37–51. PMLR.
- Vovk, V., Petej, I., Nouretdinov, I., Manokhin, V., and Gammerman, A. (2020). Computationally efficient versions of conformal predictive distributions. *Neurocomputing*, 397:292–308.
- Vovk, V., Shen, J., Manokhin, V., and Xie, M.-g. (2017). Nonparametric predictive distributions based on conformal prediction. In *Conformal and probabilistic prediction and applications*, pages 82–102. PMLR.

Proofs

Proof of Lemma 2.1

Proof. If ties occur with probability 0 (e.g. i.i.d. with a continuous law), then

$$F_n(Z_{n+1}) \sim \text{Unif}\left\{0, \frac{1}{n}, \dots, 1\right\}.$$

Let $R := \#\{i \leq [n+1] : Z_i \leq Z_{n+1}\}$ be the rank of Z_{n+1} among Z_1, \dots, Z_n, Z_{n+1} . Exchangeability gives $R \sim \text{Unif}\{1, \dots, n+1\}$. Since

$$F_{n+1}(Z_{n+1}) = \frac{R}{n+1} = \frac{n}{n+1}F_n(Z_{n+1}) + \frac{1}{n+1},$$

we get $F_n(Z_{n+1}) = \frac{R-1}{n}$, hence the discrete-uniform claim. \square

Randomized PIT under exchangeability Vovk et al. (2017)

Lemma 6.1. *Let (Z_1, \dots, Z_{n+1}) be real-valued exchangeable random variables and let $\tau \sim \text{Unif}(0, 1)$ be independent of them. Define*

$$U := (1 - \tau)F_{n+1}^-(Z_{n+1}) + \tau F_{n+1}(Z_{n+1}),$$

where F_{n+1} is the empirical CDF based on Z_1, \dots, Z_{n+1} and F_{n+1}^- is its left limit. Then

$$U \sim \text{Unif}(0, 1).$$

Proof. Condition on the multiset $\{Z_1, \dots, Z_{n+1}\}$. Let the distinct values be

$$v_1 < \dots < v_k \quad \text{with counts } m_1, \dots, m_k, \quad \sum_{j=1}^k m_j = n+1,$$

and set $S_j := \sum_{r \leq j} m_r$ (with $S_0 := 0$). Define disjoint intervals that partition $[0, 1]$:

$$I_j := \left[\frac{S_{j-1}}{n+1}, \frac{S_j}{n+1} \right], \quad |I_j| = \frac{m_j}{n+1}.$$

On the event $\{Z_{n+1} = v_j\}$, we have $F_{n+1}^-(Z_{n+1}) = \frac{S_{j-1}}{n+1}$ and $F_{n+1}(Z_{n+1}) = \frac{S_j}{n+1}$, hence the variable $U \mid (Z_{n+1} = v_j, \{Z_i\}) \sim \text{Unif}(I_j)$, since $\tau \sim \text{Unif}(0, 1)$. Furthermore, by exchangeability, conditional on $\{Z_i\}$, we have

$$\mathbb{P}(Z_{n+1} = v_j \mid \{Z_i\}) = \frac{m_j}{n+1} = |I_j|.$$

Therefore, $U \mid \{Z_i\}$ follows the mixture $\sum_{j=1}^k |I_j| \times \text{Unif}(I_j)$ and its conditional density is then

$$f_{U \mid \{Z_i\}}(u) = \sum_{j=1}^k |I_j| \cdot \frac{\mathbf{1}_{I_j}(u)}{|I_j|} = \sum_{j=1}^k \mathbf{1}_{I_j}(u) = \mathbf{1}_{[0,1]}(u).$$

Hence, for any $\alpha \in [0, 1]$,

$$\mathbb{P}(U \leq \alpha \mid \{Z_i\}) = \int_0^\alpha f_{U \mid \{Z_i\}}(u) du = \alpha.$$

Taking expectations gives $\mathbb{P}(U \leq \alpha) = \alpha$, so $U \sim \text{Unif}(0, 1)$. \square

Proof of Proposition 4.1

Proof. For $Z = Z_{n+1}$, we have by construction of the target distribution

$$\|T_{n+1}^{Z_{n+1}}(Z_{n+1})\| \sim \mathbb{U}_{n+1} \text{ supported on } \left\{0, \frac{1}{n_R}, \frac{2}{n_R}, \dots, 1\right\}$$

Here, we remind that the discrete spherical uniform distribution places the same probability mass on all $n + 1$ sample points, including the n_o copies of the origin.

As such, given a radius $r_j = \frac{j}{n_R}$, we have

$$\mathbb{P}(\|U\| = r_j) = n_S \times \frac{1}{n+1}.$$

The cumulative probability up to radius r_j is given by:

$$\mathbb{P}(\|U\| \leq r_j) = \mathbb{P}(\|U\| = 0) + \sum_{k=1}^j \mathbb{P}(\|U\| = r_k) = \frac{n_o}{n+1} + j \times \frac{n_S}{n+1}. \quad (20)$$

To find the smallest $r_\alpha = \frac{j_\alpha}{n_R}$ such that $\mathbb{P}(\|U\| \leq r_{j_\alpha}) \geq 1 - \alpha$, it suffices to solve:

$$\frac{n_o}{n+1} + j_\alpha \times \frac{n_S}{n+1} \geq 1 - \alpha.$$

□

Proof of Proposition 4.2

Proof. By excheangeability, we have $(Z_1, \dots, Z_{n+1}) \stackrel{d}{=} (Z_{\pi(1)}, \dots, Z_{\pi(n+1)})$ which implies

$$\begin{aligned} \mathbb{P}(Z_{n+1} \in \mathcal{R}_{\alpha, n+1}(Z_1, \dots, Z_{n+1})) &= \mathbb{P}(Z_{\pi(n+1)} \in \mathcal{R}_{\alpha, n+1}(Z_{\pi(1)}, \dots, Z_{\pi(n+1)})) \\ &= \mathbb{P}(Z_i \in \mathcal{R}_{\alpha, n+1}(Z_{\pi(1)}, \dots, Z_{\pi(n+1)})) \\ &= \mathbb{P}(Z_i \in \mathcal{R}_{\alpha, n+1}(Z_1, \dots, Z_{n+1})), \end{aligned}$$

where the second line follows from transitivity of the symmetric group i.e. there exists a permutation $\pi \in \mathcal{S}_{n+1}$ such that $\pi(n+1) = i$ for any $i \in [n+1]$, and finally the third line uses the permutation-invariance of the set-valued function i.e.,

$$\mathcal{R}_{\alpha, n+1}(Z_{\pi(1)}, \dots, Z_{\pi(n+1)}) = \mathcal{R}_{\alpha, n+1}(Z_1, \dots, Z_{n+1}), \quad \forall \text{ permutation } \pi.$$

Averaging over all $i \in [n+1]$ yields:

$$\begin{aligned} \mathbb{P}(Z_{n+1} \in \mathcal{R}_{\alpha, n+1}) &= \frac{1}{n+1} \sum_{i=1}^{n+1} \mathbb{P}(Z_i \in \mathcal{R}_{\alpha, n+1}) \\ &= \mathbb{E} \left[\frac{1}{n+1} \sum_{i=1}^{n+1} \mathbb{1}\{Z_i \in \mathcal{R}_{\alpha, n+1}\} \right] \\ &= \mathbb{E} [\mathbb{U}_{n+1}(\mathcal{R}_{\alpha, n+1})], \\ &\geq \mathbb{E} [1 - \alpha]. \end{aligned}$$

□

Proof of Theorem 4.1

Proof. Given any realization (Z_1, \dots, Z_{n+1}) , T_{n+1} is a permutation, so

$$\frac{1}{n+1} \sum_{i=1}^{n+1} \mathbb{1}\{T_{n+1}(Z_i) \in A\} = \frac{1}{n+1} \sum_{j=1}^{n+1} \mathbb{1}\{U_j \in A\} = \mathbb{U}_{n+1}(A). \quad (\text{E})$$

We now promote the empirical identity (E) to the population statement under $\mathbb{P}^{(n+1)}$ by invoking symmetry. Let $\pi \in S_{n+1}$ be any permutation. By exchangeability of the joint law,

$$(Z_1, \dots, Z_{n+1}) \stackrel{d}{=} (Z_{\pi(1)}, \dots, Z_{\pi(n+1)}). \quad (1)$$

Hence,

$$\mathbb{P}^{(n+1)}(T_{n+1}(Z_{n+1}; Z_1, \dots, Z_{n+1}) \in A) = \mathbb{P}^{(n+1)}(T_{n+1}(Z_{\pi(n+1)}; Z_{\pi(1)}, \dots, Z_{\pi(n+1)}) \in A). \quad (2)$$

By transitivity of the symmetric group, for any fixed $i \in [n+1]$ there exists π such that $\pi(n+1) = i$; hence

$$\mathbb{P}^{(n+1)}(T_{n+1}(Z_{\pi(n+1)}; Z_{\pi(1)}, \dots, Z_{\pi(n+1)}) \in A) = \mathbb{P}^{(n+1)}(T_{n+1}(Z_i; Z_{\pi(1)}, \dots, Z_{\pi(n+1)}) \in A). \quad (3)$$

Finally, by permutation–equivariance of the solver,

$$T_{n+1}(Z_i; Z_{\pi(1)}, \dots, Z_{\pi(n+1)}) = T_{n+1}(Z_i; Z_1, \dots, Z_{n+1}),$$

so

$$\mathbb{P}^{(n+1)}(T_{n+1}(Z_i; Z_{\pi(1)}, \dots, Z_{\pi(n+1)}) \in A) = \mathbb{P}^{(n+1)}(T_{n+1}(Z_i; Z_1, \dots, Z_{n+1}) \in A). \quad (4)$$

Combining (2)–(4) gives, for all $i \in [n+1]$,

$$\mathbb{P}^{(n+1)}(T_{n+1}(Z_{n+1}; Z_1, \dots, Z_{n+1}) \in A) = \mathbb{P}^{(n+1)}(T_{n+1}(Z_i; Z_1, \dots, Z_{n+1}) \in A).$$

Averaging over i and taking expectations of (E) yields

$$\mathbb{P}^{(n+1)}(T_{n+1}(Z_{n+1}) \in A) = \mathbb{E} \left[\frac{1}{n+1} \sum_{i=1}^{n+1} \mathbb{1}\{T_{n+1}(Z_i) \in A\} \right] = \mathbb{U}_{n+1}(A).$$

□

Proof of Proposition 4.3

Proof. Consider an arbitrary permutation $\sigma \in S_{n+1}$ that assigns sources $\{Z_1, \dots, Z_n, Z\}$ to targets $\{U_1, \dots, U_{n+1}\}$. Denote $k = \sigma(n+1)$ as the target assigned to Z . Then, for this permutation, the remaining part of the permutation σ assigns the n points Z_1, \dots, Z_n to the n remaining targets $\{U_j\}_{j \neq k}$. Since C_k is the *minimal* total cost of such an assignment, $\sum_{i=1}^n \|Z_i - U_{\sigma(i)}\|^2 \geq C_k$. Hence, the total cost of the permutation σ satisfies

$$\sum_{i=1}^n \|Z_i - U_{\sigma(i)}\|^2 + \|Z - U_k\|^2 \geq C_k + \|Z - U_k\|^2 \quad (21)$$

$$\geq C_{k^*(Z)} + \|Z - U_{k^*(Z)}\|^2 \quad (22)$$

$$= \sum_{i=1}^n \|Z_i - U_{\sigma_Z^*(i)}\|^2 + \|Z - U_{k^*(Z)}\|^2. \quad (23)$$

Hence the result.

□

Proof of Proposition 4.4

Proof. The assignment map $\psi(Z)$ selects the target point U_j minimizing

$$f_j(Z) = \|Z - U_j\|^2 + C_j,$$

where each constant C_j is precomputed from the fixed sources Z_1, \dots, Z_n . A key observation is that each cost function $f_j(Z)$ is quadratic, and the difference between two such functions is always affine: $f_k(Z) - f_j(Z) = 2\langle Z, U_k - U_j \rangle + \|U_k\|^2 - \|U_j\|^2 + C_k - C_j$. Thus, comparing $f_j(Z) \leq f_k(Z)$ is equivalent to checking a half-space condition:

$$\langle Z, U_k - U_j \rangle \leq \beta_{j,k}, \quad \text{where} \quad \beta_{j,k} := \frac{1}{2}(\|U_k\|^2 - \|U_j\|^2 + C_k - C_j).$$

The region where f_j is minimal, denoted

$$\mathcal{R}_j = \{Z \in \mathbb{R}^d : f_j(Z) \leq f_k(Z) \forall k \neq j\},$$

is thus a polyhedron defined by finitely many half-spaces, each corresponding to a pairwise comparison with another target point. Since there are only n other targets $k \neq j$, only a finite number of linear inequalities are needed to fully describe each region \mathcal{R}_j . The collection $\{\mathcal{R}_j\}_{j=1}^{n+1}$ forms a partition of \mathbb{R}^d . Each region corresponds to a fixed transport assignment: on \mathcal{R}_j , the query point Z is matched to U_j i.e. $\psi(Z) = U_j$. These regions are entirely determined by the positions of the targets and the precomputed costs C_j . Once computed, this partition is fixed and independent of Z . \square

Proof of Proposition 4.5

Proof. The target points that are interior point of the convex hull, hence we can find a contradiction if the corresponding active \mathcal{R}_j was unbounded. Indeed, assume $\mathcal{R}_j = \{Z \in \mathbb{R}^d : \langle Z, U_k - U_j \rangle \leq \beta_{j,k}, \forall k \neq j\}$ is unbounded. Then it exists a direction $v \in \mathbb{R}^d$ such that for any step $t > 0$ $\langle Z + tv, U_k - U_j \rangle \leq \beta_{j,k}$ which is only possible if

$$\langle v, U_k - U_j \rangle \leq 0 \iff U_j \in \partial \text{co}(\{U_1, \dots, U_{n+1}\}) = \partial B(0, 1)$$

which is impossible for active indices $j \in I_r$ i.e. $|U_j| \leq r < 1$ and points in the boundary of the convex hull must have a norm 1. More precisely, if \mathcal{R}_j is unbounded, then $\langle v, U_k - U_j \rangle \leq 0$ which means that U_j is in the supporting hyperplan $H_{v,j} = \{x \in \mathbb{R}^d : \langle v, x \rangle = \langle v, U_j \rangle\}$. \square

Proof of Proposition 4.6

Proof. Fix, for each l , one optimal permutation $\sigma^{(l)} \in S_{n+1}$ (if there are several, choose any), and set

$$C(\sigma) := \sum_{i=1}^n \|Z_i - U_{\sigma(i)}\|^2, \quad \psi(Z^{(l)}) := U_{\sigma^{(l)}(n+1)}.$$

Then for any $Z \in \mathbb{R}^d$ and any permutation σ , $f_\sigma(Z) = C(\sigma) + \|Z - U_{\sigma(n+1)}\|^2$.

Cyclical monotonicity. Let $\sigma^{(m+1)} := \sigma^{(1)}$. By optimality of $\sigma^{(l)}$ for the problem with query $Z^{(l)}$, we have, for each $l = 1, \dots, m$,

$$C(\sigma^{(l)}) + \|Z^{(l)} - \psi(Z^{(l)})\|^2 \leq C(\sigma^{(l+1)}) + \|Z^{(l)} - \psi(Z^{(l+1)})\|^2.$$

Summing over $l \in [m]$ and using that $\sum_{l=1}^m C(\sigma^{(l)}) = \sum_{l=1}^m C(\sigma^{(l+1)})$ (a cyclic reindexing) yields

$$\sum_{l=1}^m \|Z^{(l)} - \psi(Z^{(l)})\|^2 \leq \sum_{l=1}^m \|Z^{(l)} - \psi(Z^{(l+1)})\|^2,$$

which is the desired cyclical monotonicity.

Indeed, since $\sigma^{(m+1)} := \sigma^{(1)}$, it holds

$$\sum_{l=1}^m C(\sigma^{(l+1)}) = \sum_{l=2}^{m+1} C(\sigma^{(l)}) = \sum_{l=2}^m C(\sigma^{(l)}) + C(\sigma^{(m+1)}) = \sum_{l=1}^m C(\sigma^{(l)}).$$

Monotonicity. Taking $m = 2$ in the previous inequality gives

$$\|Z^{(1)} - \psi(Z^{(1)})\|^2 + \|Z^{(2)} - \psi(Z^{(2)})\|^2 \leq \|Z^{(1)} - \psi(Z^{(2)})\|^2 + \|Z^{(2)} - \psi(Z^{(1)})\|^2.$$

Expanding squared norms and cancelling identical terms on both sides yields

$$\langle Z^{(1)} - Z^{(2)}, \psi(Z^{(1)}) - \psi(Z^{(2)}) \rangle \geq 0,$$

which is the standard (pairwise) monotonicity of the map $Z \mapsto \psi(Z)$. \square

Proof of Theorem 5.1

Proof. We have i.i.d. auxiliary seeds $(\tau_i)_{i=1}^{n+1}$, independent of the data.

(E) Empirical identity. By definition of the randomized kernel, for each i and any $B \subseteq Y$,

$$\mathbb{E}[\mathbb{1}\{\tilde{T}_{n+1}(Z_i, \tau_i) \in B\} \mid Z_1, \dots, Z_{n+1}] = \mathbb{U}_{\sigma^*(i)}(B). \quad (24)$$

Averaging (24) over $i = 1, \dots, n+1$ and using that σ^* is a bijection and $\mathbb{U}(A_k) = 1/(n+1)$,

$$\begin{aligned} \frac{1}{n+1} \sum_{i=1}^{n+1} \mathbb{U}_{\sigma^*(i)}(B) &= \frac{1}{n+1} \sum_{k=1}^{n+1} \mathbb{U}_k(B) = \frac{1}{n+1} \sum_{k=1}^{n+1} \frac{\mathbb{U}(B \cap A_k)}{\mathbb{U}(A_k)} \\ &= \sum_{k=1}^{n+1} \mathbb{U}(B \cap A_k) = \mathbb{U}(B). \end{aligned} \quad (E')$$

This step is purely empirical: it relies only on the equal-mass partition and the definition of the kernel, not on pushing \mathbb{P} forward, which is anyway unknown in practice.

(X) Going to population statement Fix a set B . We now promote the empirical identity to a population statement for the held-out point, using exchangeability and permutation–equivariance.

(X1) Exchangeability. For any permutation $\pi \in \mathcal{S}_{n+1}$,

$$(Z_1, \dots, Z_{n+1}) \stackrel{d}{=} (Z_{\pi(1)}, \dots, Z_{\pi(n+1)}). \quad (25)$$

Hence,

$$\mathbb{P}^{(n+1)}(\tilde{T}_{n+1}(Z_{n+1}; Z_1, \dots, Z_{n+1}) \in B) = \mathbb{P}^{(n+1)}(\tilde{T}_{n+1}(Z_{\pi(n+1)}; Z_{\pi(1)}, \dots, Z_{\pi(n+1)}) \in B). \quad (26)$$

(X2) Transitivity. For any fixed $i \in [n+1]$, choose π with $\pi(n+1) = i$. Then (26) gives

$$\mathbb{P}^{(n+1)}(\tilde{T}_{n+1}(Z_{n+1}; Z_1, \dots, Z_{n+1}) \in B) = \mathbb{P}^{(n+1)}(\tilde{T}_{n+1}(Z_i; Z_{\pi(1)}, \dots, Z_{\pi(n+1)}) \in B). \quad (27)$$

(X3) Permutation–equivariance. By permuting the label of the points, the OT maps does not changes, thus the distribution of the image of Z_i is invariant under relabeling the dataset:

$$\tilde{T}_{n+1}(Z_i; Z_{\pi(1)}, \dots, Z_{\pi(n+1)}) = \tilde{T}_{n+1}(Z_i; Z_1, \dots, Z_{n+1}). \quad (28)$$

Combining (27)–(28), for every $i \in [n + 1]$,

$$\mathbb{P}^{(n+1)}(\tilde{T}_{n+1}(Z_{n+1}; Z_1, \dots, Z_{n+1}) \in B) = \mathbb{P}^{(n+1)}(\tilde{T}_{n+1}(Z_i; Z_1, \dots, Z_{n+1}) \in B). \quad (29)$$

Now, averaging (29) over $i = 1, \dots, n + 1$ and applying the tower property together with (24)–(E'), we obtain

$$\begin{aligned} \mathbb{P}^{(n+1)}(\tilde{T}_{n+1}(Z_{n+1}, \tau) \in B) &= \frac{1}{n+1} \sum_{i=1}^{n+1} \mathbb{P}^{(n+1)}(\tilde{T}_{n+1}(Z_i, \tau_i) \in B) \\ &= \mathbb{E} \left[\frac{1}{n+1} \sum_{i=1}^{n+1} \mathbb{E} \left[\mathbf{1} \{ \tilde{T}_{n+1}(Z_i, \tau_i) \in B \} \mid Z_1, \dots, Z_{n+1} \right] \right] \\ &= \mathbb{E} \left[\frac{1}{n+1} \sum_{i=1}^{n+1} \mathbb{U}_{\sigma^*(i)}(B) \right] = \mathbb{E}[\mathbb{U}(B)] = \mathbb{U}(B), \end{aligned}$$

which is the desired identity. \square

Proof of Proposition 5.1

Proof. Step 1: Reduction to an assignment over cells. Because $\mathbb{U}(A_k) = 1/(n + 1)$ for all k and the source points each have mass $1/(n + 1)$, any feasible plan from the augmented source to \mathbb{U} that adapt to the cell structure, i.e. only sends mass into the partition $\{A_k\}$, corresponds to a nonnegative matrix $P = (p_{ik})_{i \in [n+1], k \in [n+1]}$ with row sums 1 and column sums 1:

$$p_{ik} \text{ is the fraction of point } \zeta_i \text{ routed to cell } A_k, \quad \sum_k p_{ik} = 1, \quad \sum_i p_{ik} = 1.$$

The transport cost of such a plan is

$$\frac{1}{n+1} \sum_{i,k} p_{ik} \int_{A_k} \|\zeta_i - u\|^2 d\mathbb{U}_k(u) = \frac{1}{n+1} \sum_{i,k} p_{ik} \bar{c}(\zeta_i, k).$$

The feasible set $\{P \geq 0 : P\mathbf{1} = \mathbf{1}, P^\top \mathbf{1} = \mathbf{1}\}$ is the Birkhoff polytope; its extreme points are permutation matrices (Birkhoff–von Neumann theorem). Since the objective is linear in P , an optimal plan exists at an extreme point, i.e., at a bijection $\tilde{\sigma}$ with cost

$$\frac{1}{n+1} \sum_{i=1}^{n+1} \bar{c}(\zeta_i, \tilde{\sigma}(i)) = \frac{1}{n+1} \left(\sum_{i=1}^n \bar{c}(Z_i, \tilde{\sigma}(i)) + \bar{c}(Z, \tilde{\sigma}(n+1)) \right).$$

Thus minimizing over adapted plans is equivalent to minimizing over bijections $\tilde{\sigma}$.

Step 2: Decomposition and the precomputed constants C_k . Fix any bijection $\tilde{\sigma}$ and write $k := \tilde{\sigma}(n + 1)$. Then

$$\begin{aligned} \sum_{i=1}^n \bar{c}(Z_i, \tilde{\sigma}(i)) + \bar{c}(Z, k) &\geq \min_{\sigma: [n] \rightarrow [n+1] \setminus \{k\}} \sum_{i=1}^n \bar{c}(Z_i, \sigma(i)) + \bar{c}(Z, k), \\ &= C_k + \bar{c}(Z, k) \end{aligned}$$

with equality achieved by choosing $\tilde{\sigma}$ whose restriction to $[n]$ attains C_k . Thus the optimal augmented cost is

$$\min_{k \in [n+1]} \{ \bar{c}(Z, k) + C_k \} = \min_k f_k(Z),$$

and any bijection σ_Z^* constructed as in the statement attains this minimum.

Step 3: Optimality of the randomized transport. Let σ_Z^* be such a bijection. Because exactly one source point is assigned to each cell A_k and the target marginal must equal \mathbb{U} , the only way

to realize the correct second marginal on A_k is to send that point with the *conditional* law \mathbb{U}_k . Therefore the coupling

$$\pi^* = \frac{1}{n+1} \sum_{i=1}^{n+1} \delta_{\zeta_i} \otimes \mathbb{U}_{\sigma_Z^*(i)}$$

is feasible and attains the assignment cost in eq. (19). By Step 1, an optimal coupling exists at a permutation and the cost is linear in the coupling, hence π^* is optimal.

Step 4: Polyhedral decision regions. From (16) and (18),

$$\begin{aligned} f_k(Z) - f_\ell(Z) &= (\|Z\|^2 - 2\langle Z, m_k \rangle + s_k + C_k) - (\|Z\|^2 - 2\langle Z, m_\ell \rangle + s_\ell + C_\ell) \\ &= -2\langle Z, m_k - m_\ell \rangle + (s_k - s_\ell) + (C_k - C_\ell). \end{aligned}$$

Thus $\{Z : f_k(Z) \leq f_\ell(Z)\}$ is a half-space bounded by an affine hyperplane, and

$$\mathcal{R}_k = \bigcap_{\ell} \{Z : f_k(Z) \leq f_\ell(Z)\}$$

is a convex polyhedron.

Verification that π_Z^* pushes μ_Z to \mathbb{U} (for every Z) It suffices to check the two marginals. To see that the first marginal equals μ_Z , we have by construction,

$$(\pi_Z^*)_1 = \frac{1}{n+1} \sum_{i=1}^{n+1} \delta_{\zeta_i} = \mu_Z.$$

Let's see that the second marginal equals \mathbb{U} . Since σ_Z^* is a bijection of $[n+1]$,

$$(\pi_Z^*)_2 = \frac{1}{n+1} \sum_{i=1}^{n+1} \mathbb{U}_{\sigma_Z^*(i)} = \frac{1}{n+1} \sum_{k=1}^{n+1} \mathbb{U}_k.$$

But $\mathbb{U}_k = \mathbb{U}(\cdot | A_k) = \mathbb{U}(\cdot \cap A_k) / \mathbb{U}(A_k)$ and $\mathbb{U}(A_k) = 1/(n+1)$, hence

$$\frac{1}{n+1} \sum_{k=1}^{n+1} \mathbb{U}_k(\cdot) = \frac{1}{n+1} \sum_{k=1}^{n+1} \frac{\mathbb{U}(\cdot \cap A_k)}{1/(n+1)} = \sum_{k=1}^{n+1} \mathbb{U}(\cdot \cap A_k) = \mathbb{U}(\cdot).$$

Therefore $(\pi_Z^*)_2 = \mathbb{U}$. □

Proof of Proposition 5.2

Proof. For each l , optimality of $\sigma^{(l)}$ for the augmented problem with query $Z^{(l)}$ yields

$$\sum_{i=1}^n \bar{c}(Z_i, \sigma^{(l)}(i)) + \bar{c}(Z^{(l)}, \sigma^{(l)}(n+1)) \leq \sum_{i=1}^n \bar{c}(Z_i, \sigma^{(l+1)}(i)) + \bar{c}(Z^{(l)}, \sigma^{(l+1)}(n+1)),$$

that is,

$$C_{k_l} + \bar{c}(Z^{(l)}, k_l) \leq C_{k_{l+1}} + \bar{c}(Z^{(l)}, k_{l+1}).$$

Summing over $l = 1, \dots, m$ and using $\sum_{l=1}^m C_{k_l} = \sum_{l=1}^m C_{k_{l+1}}$ (a cyclic reindexing) gives

$$\sum_{l=1}^m \bar{c}(Z^{(l)}, k_l) \leq \sum_{l=1}^m \bar{c}(Z^{(l)}, k_{l+1}),$$

which is statement (i), since $\bar{c}(Z, k) = \mathbb{E}\|Z - U\|^2$ for $U \sim \mathbb{U}(\cdot | A_k)$.

For (ii), take $m = 2$ and expand \bar{c} using $\bar{c}(z, k) = \|z\|^2 - 2\langle z, m_k \rangle + s_k$:

$$\begin{aligned} & (\|Z^{(1)}\|^2 - 2\langle Z^{(1)}, m_{k_1} \rangle + s_{k_1}) + (\|Z^{(2)}\|^2 - 2\langle Z^{(2)}, m_{k_2} \rangle + s_{k_2}) \\ & \leq (\|Z^{(1)}\|^2 - 2\langle Z^{(1)}, m_{k_2} \rangle + s_{k_2}) + (\|Z^{(2)}\|^2 - 2\langle Z^{(2)}, m_{k_1} \rangle + s_{k_1}). \end{aligned}$$

Cancelling identical terms on both sides yields

$$-2\langle Z^{(1)}, m_{k_1} \rangle - 2\langle Z^{(2)}, m_{k_2} \rangle \leq -2\langle Z^{(1)}, m_{k_2} \rangle - 2\langle Z^{(2)}, m_{k_1} \rangle,$$

or equivalently

$$\langle Z^{(1)} - Z^{(2)}, m_{k_1} - m_{k_2} \rangle \geq 0,$$

which is the desired pairwise monotonicity for $\phi_{\text{sd}}(Z) = m_{k^*(Z)}$. \square

Proof of Proposition 5.3

Proof. Fix k with $A_k \subseteq B(0, r)$ and suppose, by contradiction, that \mathcal{R}_k is unbounded. By Proposition 5.1,

$$\mathcal{R}_k = \bigcap_{\ell \neq k} \{Z : f_k(Z) \leq f_\ell(Z)\} = \bigcap_{\ell \neq k} \left\{ Z : \langle Z, m_\ell - m_k \rangle \leq \frac{1}{2}(s_\ell - s_k + C_\ell - C_k) \right\},$$

where $m_j = \int u d\mathbb{U}(u | A_j)$ and $s_j = \int \|u\|^2 d\mathbb{U}(u | A_j)$. If \mathcal{R}_k were unbounded, there would exist a nonzero direction v such that

$$\langle v, m_\ell - m_k \rangle \leq 0 \quad \forall \ell,$$

so that the linear form $u \mapsto \langle v, u \rangle$ attains its maximum over the finite set $\{m_1, \dots, m_{n+1}\}$ at m_k . Because the Laguerre cells $\{A_\ell\}$ partition the entire unit ball and cover all directions, there exists an index $\ell(v)$ whose cell intersects the spherical cap $\{u = tv/\|v\| : t \in (\rho, 1]\}$ for some $\rho < 1$. Then

$$\langle v, m_{\ell(v)} \rangle \geq \sup_{u \in A_{\ell(v)}} \langle v, u \rangle - \varepsilon \geq \rho\|v\| - \varepsilon,$$

for arbitrarily small $\varepsilon > 0$, while $A_k \subseteq B(0, r)$ implies $\langle v, m_k \rangle \leq r\|v\|$. Choosing $\rho \in (r, 1)$ and ε small gives $\langle v, m_{\ell(v)} \rangle > \langle v, m_k \rangle$, contradicting the maximality of $\langle v, m_k \rangle$. Hence \mathcal{R}_k must be bounded. Since Ω_r^{sd} is a finite union of such regions, it is bounded. \square